7471-EN-09
DTIC

AD

REPORT 26-04-R-09

EARTHQUAKE INDUCED LIQUEFACTION OF CONFINED ZONES

PHASE 3

FINAL TECHNICAL REPORT

by

R S Steedman

1 April 1997

United States Army

EUROPEAN RESEARCH OFFICE OF THE U.S. ARMY

London, England

CONTRACT NUMBER N68171-94-C-9120

ANDREW N SCHOFIELD & ASSOCIATES LTD
9 LITTLE ST MARYS LANE
CAMBRIDGE CB2 1 RR, U.K.

REPORT DOCUMENTATION PAGE

Contract No:	N68171-94-C-9120
Title of Proposal	Earthquake induced liquefaction of confined zones: Phase 3
Name of Institution	Andrew N Schofield & Associates Ltd 9 Little St Marys Lane Cambridge CB2 1RR, U.K.
Principal Investigator	Dr R Scott Steedman

R S Steedman

1 April 1997

SUMMARY

This report presents an analysis of a series of centrifuge earthquake model experiments conducted at Cambridge University, England, on sand embankments incorporating a zone of poorly compacted 'loose' material. The experiments were designated GEM 1 to GEM 6 and were carried out at the Cambridge Geotechnical Centrifuge Centre using the bumpy road earthquake actuator on the beam centrifuge during 1992-1993.

In this report, data from the model experiments is reviewed and analysed under a number of key headings : excess pore pressure development, embankment response, natural frequencies and phase differences, and mechanisms of failure.

The report concludes that loose zones within an otherwise dense embankment will facilitate the development of gross deformations during and after seismic shaking. The predominant direction of down-slope movement was in all cases towards the side of the embankment with the loose pocket or zone, although shallow slides were also observed in several cases on the opposite, dense side of the embankment. The shape of the loose zone is a significant factor, as is the extent to which residual excess pore pressures can develop and be maintained during and following shaking.

Different techniques were used to form and to encapsulate the loose zones. A freezing technique was developed which proved effective in avoiding densification of the loose pocket prior to the start of the experiment but was restricted to experiments which used water as a pore fluid. Novel techniques were also developed to encapsulate the loose zone, restricting the ability of high excess pore pressures to drain rapidly, using water saturated sheets of lasagne to provide a low strength impermeable boundary, or sheets of silicon rubber commonly used for membranes in laboratory element testing.

The response of the embankments was dramatically different in the four later oil-saturated models compared to the initial two water saturated models. In the first models, which had relatively small loose zones, there was evidence of liquefaction but the dominant response of the embankment was in phase with the base shaking, exhibiting settlements and compaction with some slumping towards the side of the embankment with the loose pocket.

In the four later models, extensive liquefaction took place throughout the embankments, both in the loose zones and in the denser sections. Very high residual pore pressures were maintained in the loose zones well beyond the completion of any down-slope movement. Large scale gross deformations were observed towards the loose side in all four cases, with evidence of deep seated mechanisms being invoked for part of this period. Shallow down-slope movements were also observed on the dense side of the embankment. In several cases, there is evidence that movement continued after the main shaking had finished, associated with 'aftershock' cycles of shaking.

LIST OF KEYWORDS

liquefaction
centrifuge
model
test
embankment
earthquake
slope
seismic
acceleration
pore pressure
dynamic response

CONTENTS

LIST OF TABLES

1. INTRODUCTION

Earth dams, embankments and levées are an important and widely used form of civil engineering construction. Under seismic loading, such structures often perform satisfactorily (with damage limited to settlements and minor surface movements) but occasionally large scale slides or collapses have been observed which have caused disproportionate and unacceptable levels of damage. In such cases, this behaviour can often be linked to the development of high excess pore pressures and/or liquefaction of loose materials either within or beneath the structure. Such loose pockets or zones may have been created during construction, or they may occur naturally in the foundation and have been ignored or overlooked in the original design.

During an earthquake soil elements in the embankment are subject to rapidly cycling shear stress and rotation of the principal stress direction. In the case of an initially loose soil element this will lead to densification of the zone causing (in saturated ground) an instantaneous rise in pore pressure (followed by consolidation). The rise in excess pore pressure leads to a reduction in the effective confining stress, reducing the strength and stiffness of the material. As the excess pore pressure approaches the total confining pressure a condition known as initial liquefaction may result which, if sustained by high hydraulic gradients can lead to the break-up of the continuum, near-total loss of strength and large scale deformations.

As part of a wider research program into the implications of confined and unconfined loose zones on the seismic design and remediation of earth dams a series of centrifuge earthquake model experiments were carried out in 1992[1] and 1993[2] at Cambridge University, England, using the large beam centrifuge at the Cambridge Geotechnical Centrifuge Centre, Schofield (1980)[3]. The principles of dynamic and earthquake centrifuge modelling have been described in detail elsewhere, see for example Schofield (1981)[4], and are therefore not addressed here. The details of the earthquake actuator system were described by Kutter (1983)[5].

---

[1] Steedman R S and Madabushi S P G (1992), Earthquake-induced liquefaction of confined soil zones: a centrifuge study, Final Technical Report, USARDSG-UK, Contract DAJA45-92-C-0022.
[2] Steedman R S and Madabushi S P G (1993), Earthquake-induced liquefaction of confined soil zones: a centrifuge study, Final Technical Report, USARDSG-UK, Contract DAJA45-93-C-0029.
[3] Schofield AN (1980), Cambridge Geotehnical Centrifuge Operations, Geotechnique, Vol 25, No 4, pp 743-761.
[4] Schofield AN (1981), Dynamic and earthquake geotechnical centrifuge modelling, Proc. Int. Conf. Recent Advances Geotech. Earthquake Eng Soil Dynamics, Vol. 3, pp 1081-1100, Univ. Missouri Rolla.
[5] Kutter BL (1982), Centrifugal modelling of the response of clay embankments to earthquakes, PhD thesis, Cambridge University, England.

The experiments were designated GEM 1 through GEM 6. In the sections below, the experiments are broken down into two main groups, GEM 1 and GEM 2, and GEM 3 to 6.

2. INITIAL STUDIES USING WATER AS A PORE FLUID

For the initial model experiments, water was used as a pore fluid primarily to simplify model construction and to create an initial dataset from which more complex model experiments could be developed. Later sections of this report describe four experiments which followed these initial two models.

Two grades of sand were used in the construction of all the models, including the initial model experiments. Leighton Buzzard 52/100 sand placed medium dense was used to form the dense section of the levées or embankments. It had a specific gravity of 2.65 and maximum and minimum void ratios of 0.980 and 0.585 respectively. The loose pocket was constructed using a fine grained Nevada sand with a specific gravity of 2.68, a maximum void ratio of 0.894 and a minimum void ratio of 0.516. De-ionised water was used as the pore fluid for the two initial model tests, designated GEM 1 and GEM 2.

In order to prevent densification of the loose zone due to disturbance during transfer from the model preparation room to the centrifuge arm a new technique was developed for these experiments whereby the loose zone was constructed outside the model, saturated, frozen and then placed in the model as a single block. The loose material was kept in its frozen condition by a heat pump system while the denser material was placed around it. The heat pumps were turned off once the model had been securely mounted on the centrifuge arm. Further details concerning the experimental procedures and the use of the Peltier Heat Pump Array (PHPA) are given in the 1992 data report.

The heat pump array system proved effective in maintaining the quality or density of the loose zone of Nevada sand and there was no evidence of disturbance to the loose pocket during the model preparation or during transportation onto the centrifuge arm. Its major deficiency is that for the freezing technique to work water must be used as the pore fluid, restricting the capability to retain excess pore pressures in the model generated during shaking.

The accelerations in the soil and on the strong box model container were measured using miniature piezoelectric accelerometers manufactured by D J Birchall. Similarly pore pressures in the saturated soil were monitored by Druck PDCR 81 pore pressure transducers. The GEM 2 test differed from GEM 1 in that it incorporated a differential hydraulic head across the embankment which was achieved by use of a vertical rubber sheet or membrane at the 'upstream' shoulder to create a barrier to flow.

A total of three earthquakes were fired in test GEM 1 and two in GEM 2. All earthquakes were fired at 80g. The amplitude of the earthquakes was gradually increased during each flight; for GEM 1 peak base inputs (at the base of the embankment) were 5.9%, 9.7% and 11.5% and for GEM 2, peak mean base inputs were 23.1% and 25.6%.

2.1 Development of excess pore pressures

Two pore pressure transducers were located in the loose pocket in model GEM 1; PPT 6518 was located towards the bottom of the loose pocket, while PPT 3156 was positioned higher up and closer to the slope. PPT 6518 showed a steady build up of excess pore pressure in earthquake 1 with little cyclic response, reaching a peak residual value of around 12 KPa. Table 1 shows a calculation of $\Delta u/\sigma_v'$ for peak and residual excess pore pressure from which it is clear that levels of excess pore pressure in earthquake 1 were not sufficient to achieve liquefaction. These excess pore pressures dissipated rapidly after shaking, as expected. However, during earthquake 2 and particularly in earthquake 3 the underlying residual pore pressure is reduced compared to earthquake 1 and the behaviour is dominated by a large cyclic response at double the frequency of the strong motion input. The other transducer, near the top of the loose zone (PPT 3156), also showed some residual rise in pore pressure in earthquake 1 but the dominant behaviour at this location was large cycling of excess pore pressure at the main earthquake shaking frequency.

One of the most significant results shown by these traces is the evidence for densification. Densification is most obvious for PPT 6518 which shows a progressive change in behaviour from earthquake 1 to earthquake 3. By earthquake 3 sufficient densification has occurred that only a small residual positive excess pore pressure is generated, especially noting that the amplitude of the earthquake has significantly increased. Comparison between earthquake 1 and earthquake 3 for PPT 3156 also shows a similar pattern. Comparison between PPT 6518 and PPT 3156 shows the influence of longer drainage paths.

The generation of cyclic pore pressures can be explained using the conceptual framework of Habib (1978)[6] which is also outlined in Lee and Schofield (1988)[7]. Cyclic variation in deviator stress causes a steady build up of pore pressures and a reduction in effective stress. If the static deviator stress is small pore pressures may rise substantially before the characteristic stress ratio is reached (Lee and Schofield).

[6] Habib P and Luong MP (1978), Sols pulverulents sous chargement cyclique, *Materieux et structures sous chargement cyclique*, pp 49-79, Palaiseau: Association Amicale des Ingenieurs Anciens Eleves de l'Ecole Nationale des Ponts et Chaussees.

[7] Lee FH and Schofield AN (1988), Centrifuge modelling of sand embankments and islands in earthquakes, Geotechnique **38**, No 1, pp 45-58.

This sort of behaviour is illustrated by PPT 6518. However if significant deviator stress is present the characteristic stress ratio may be reached with a smaller pore pressure increase. At the characteristic ratio pore pressures fluctuate cyclically but there is no mean pore pressure rise, as shown by PPT 3156.

This same model explains the observation of double frequency pore pressure generation at PPT 6518. Once the characteristic state has been reached the stress path can either lead to liquefaction or to cyclic mobility. The double frequency response is seen at PPT 6518 rather than PPT 3156 because the static shear stress at PPT 6518 is much lower than at PPT 3156, which is in the exposed slope.

The pore pressure transducers in the dense sand on the same side as the loose zone showed the generation of excess pore pressures at the same frequency as the strong motion input. Both PPTs 6269 and 6270 showed generally symmetrical cycles with peak values approximately proportional to the magnitude of the input in the different events.

PPT 6517 at the base of the embankment in the core also shows strongly cyclical behaviour during earthquake 1 (with a build-up of excess pore pressure), but an increasing tendency towards negative 'spikes' of pore pressure and an overall negative residual pressure (indicating dilation) towards the end of the strong motion in both earthquake 2 and earthquake 3, which is difficult to explain. In earthquake 3 in particular, PPT 6517 shows large sharp negative pulses near the start of shaking, disproportionate to the level of shaking, and later shows some double frequency response, flat peaks and a long period of residual negative pressure after the shaking has finished. These data (earthquake 3 and possibly also earthquake 2) should be treated with caution.

Also in the central core, PPT 6560 (at mid-depth) showed strongly cyclic behaviour, again at the driving or input frequency, and some generation of residual positive excess pore pressure (which dissipated rapidly when the input motion ceases). The cycles of excess pore pressure are broadly symmetric during earthquake 1, but show an increasing tendency in earthquake 2 and clearly in earthquake 3 towards asymmetric behaviour, probably linked to downslope movement on the dense side, with 'flat' positive peaks the onset of which roughly coincide with the end of each period of downslope movement, as evidenced by the mid-slope accelerometer, ACC5701.

Out on the slope on the dense side of the embankment PPT 6159 (the only PPT on this side for which data is reproduced) also showed cyclic pore pressures fluctuating at the same frequency as the base input but 180^{o} out of phase with the other PPTs in all three earthquakes. During earthquake 1 these cycles are roughly symmetric but in earthquakes 2

and 3 this behaviour becomes strongly asymmetric as a high residual excess pore pressure is interrupted by sharp negative increments appearing to coincide with episodes of downslope movement (indicating shearing and dilation) which can be deduced from ACC 5701 and observations made at the end of the three strong motion inputs (see below).

Following Newmark (1965)[8] a quasi-static lateral acceleration field will be capped at the onset of movement in sliding at a limiting or threshold acceleration, associated with the strength of the slope, the applied loads and the geometry. The movement will continue until the velocities of the sliding elements and the underlying ground are again identical, during which time the acceleration of the sliding elements is constant or near constant (depending on the kinematic constraints). ACC 5701 shows a marked asymmetric response, with negative accelerations capped at around -4.5% (+/- 1%). The periods over which the negative accelerations are capped correlates closely with the periods of sharply dropping excess pore pressure at PPT 6159. Once the down-slope movement stops, the pore pressures quickly build up again to a high positive residual value.

The phase difference of 180° between PPT 6159 and the other transducers is due simply to its location on the opposite side of the embankment to the other devices. Lee and Schofield describe the mechanism by which an acceleration up-slope and down-slope lead to alternate dilation and contraction, cycling up and down the characteristic threshold. In the embankment, when one side is accelerated upwards, the same motion is driving the opposite slope downwards, leading to the opposite mode of behaviour in pore pressure response. The spikey acceleration records which are associated with this behaviour (note the sharp positive pulses in ACC 5701) were also discussed by Lee and Schofield, and explained as being related to the crossing of the stress point onto the dry side of the characteristic line, generating sudden, rapid dilation.

The location of instrumentation in GEM 2 was broadly similar to that for GEM 1, allowing for differences due to the effect of the vertical membrane.

In GEM 2 both the PPTs in the loose zone (PPT 6518 and PPT 3156) showed a rapid build up of positive excess pore pressures in the two earthquakes with flat tops providing clear evidence of excess pore pressures reaching 100% of the insitu overburden effective stress (initial liquefaction). Although not located as deep as in GEM 1, the deeper of the two transducers in GEM 2, PPT 6518, showed a cyclic

[8] Newmark NM (1965), Effect of Earthquakes on Dams and Embankments, Geotechnique, Vol 15, No 2, pp 139-160.

response at the main driving frequency in both events (not the double frequency response observed in GEM 1). The build up of positive excess pore pressures in both PPT 6518 and PPT 3156 which is maintained throughout the strong motion input indicates that the zone was functioning as a 'generator' of excess pore pressure throughout both events.

There is little difference between the overall pattern of pore pressure response in earthquake 1 and 2 with the exception of the PPTs in the core, PPT 3139 and PPT 3000 whose response changed in character, as if a static shear stress had been released at the end of earthquake 1. The amplitude of the response in both cases was very small, compared to similar locations in GEM 1, but the similar character of the two records suggests that they are probably recording real phenomena. In earthquake 1, both show a modest increase and then cycling at the driving frequency. In earthquake 2, no residual is seen, and cycling takes place at twice the driving frequency from early in the event.

The observed double frequency reponse in earthquake 2 is surprising, given the overburden stress. It may be possible that their behaviour has been affected by the membrane between the 'upstream' and 'downstream' sections of the embankment, which may have inhibited the generation and drainage of excess pore pressures. This could be because it has affected the placement of the soil, or because it has provided an essentially frictionless vertical wound, distorting the pattern of shear stress in the embankment.

The pore pressure transducers in each toe of the embankment, PPT 6264 on the 'upstream' side with the loose pocket, and PPT 6513 on the dense side, both show strong cyclic behaviour. There is some evidence, from close examination of PPT 6264, of a 'flat top' to the positive pore pressures at about half the peak (negative) value in earthquake 1 and at a slightly higher absolute value in earthquake 2 (around 4-5 KPa) indicating initial liquefaction in both earthquakes, possibly with the transducer being more deeply buried in earthquake 2 than in earthquake 1. Measurements taken after the experiment provide evidence for such a failure.

The remaining transducer on the dense side of the embankment (PPT 6261) also showed a largely symmetric response without the development of any residual pore pressure. Some rounding of the positive peaks and the slightly shark's tooth character of the nearby accelerometer (ACC 3466) suggests that some minor movement did take place, but negligible in comparison to GEM 1.

2.2 Dynamic response in water saturated models

In GEM 1 the magnitude of the base input accelerations was 6% g, 10% g and 12% g in earthquakes 1 to 3 respectively. Table 2 shows the relative amplification between the base and each transducer, based on the maximum and minimum values recorded.

Seven accelerometers, one in the loose zone six in the relatively dense zone, recorded the behaviour of the embankment. Accelerometer ACC 1552 at the base of the embankment indicates a highly symmetric shaking, with minimum noise, and is therefore considered to provide an ideal reference for the model tests. ACC 3436 near the base on the dense side shows a similar character of response, with no significant amplification. Near the toe at the base on the opposite side (the side with the loose pocket) ACC 3441 showed a more ragged response, with significant higher frequencies but again, no significant amplification.

The accelerometer at the top of the loose zone (ACC 5754) showed a very regular response, with little amplification (Table 2), closely following the base of the embankment in all earthquakes. In the larger earthquakes 2 and 3, some slight rounding of the peaks (giving a shark's teeth appearance) indicates movement, probably densification.

Two of the three accelerometers in the dense central core were affected by electrical problems. The base line for ACC 1932 in earthquakes 2 and 3 seemed to drift, distorting the maximum and minimum auto-calculated values. Although unfortunate, the peak to peak values can be used rather than the absolute values to determine amplification. These are shown as 'corrected values' in Tables 2, 3 and 4. In all three earthquakes, strong amplification appears to have occurred near this device, in the centre of the embankment (ACC 1932). However, this is not consistent with the data from ACC 1572, which is located above ACC 1932, also in the core of the embankment. Although ACC 1572 did not perform fully during earthquake 1 (and is not reported for earthquakes 2 and 3), it does not show the same amplification as appears to have been observed at ACC 1932. The output from both devices should be treated with caution.

Reference has been made above to the data from ACC 5701 on the dense side of the embankment. Although this shows an anomaly towards the end of earthquake1 it shows clear evidence of downslope movement in earthquake 2 and earthquake 3, on the opposite side of the embankment to the loose pocket. This is supported by the trace from the adjacent pore pressure transducer PPT 6159. Measurements of the surface profile after the three strong motion inputs also support the interpretation that the failure is a shallow surface slip.

The generally low level of amplification at all accelerometers except ACC 1932, Tables 2, 3 and 4, further supports the conclusion that the absolute level of acceleration at ACC 1932 is probably in error.

The mean peak amplitude of the input accelerations at the base of the embankment in GEM 2 was around 21% g and 24% g in earthquakes 1 and 2, respectively, based on ACC 3477.

All accelerometers showed broadly symmetric behaviour closely correlated to the input motion, with no clear indication of sliding occurring due to the movement of discrete blocks of soil. However, on the slope of the embankment on the dense side, a slight smearing of the peaks of the acceleration records suggests some movement, probably settlement and spreading (ACC 3466 and ACC 3436). It should be noted that there were no accelerometers on the side of the embankment with the loose pocket, which is the side determined by slope stability calculations to be more critical, Appendix A. Observations afterwards indicate that large settlements of the crest did occur, but there was no noticeable heave on either side of the embankment.

ACC 5717 in the dense central core of the embankment showed a baseline drift, but this has not otherwise affected the quality of the signal. As with the data from GEM 1, the exceptionally high values of acceleration recorded at ACC 1932 suggest that the absolute values are in error, but this notwithstanding, the qualitative information from the accelerometer is consistent with the nearby devices ACC 3466 and ACC 3436 and therefore remains of some value.

Amplifications were again modest, with the peak values being observed at or near the crest (neglecting ACC 1932 for the reasons given above), and clearly greater in one sense as opposed to the other, ie. showing evidence of some asymmetric response, Tables 5 and 6.

2.3 Natural frequency

The natural frequency of the embankments modelled in GEM 1 and GEM 2 has been calculated after Ambraseys (1960)[9] and the results are presented in Table 7. The embankment was considered as a two dimensional elastic wedge subject to an imposed horizontal unidirectional time dependent disturbance which generated deflections and shears in the wedge. The dynamic stiffness of the sand was determined following Hardin and Drnevich (1972)[10]. The disturbance was considered to act normally to the longitudinal plane of symmetry

[9] Ambraseys NN (1960), On the shear response of a two dimensional truncated wedge subjected to an arbitrary disturbance, Bulletin of the Seismological Society of America, Vol 50, No 1, pp 45-56.
[10] Hardin BO and Drnevich VP (1972), Shear modulus and damping in soils: design equations and curves, Journal of the Soil Mechanics and Foundations Division, Proc ASCE, SM7, pp 667-692.

of the wedge which was considered to be perfectly elastic and symmetrical, bounded at its base and on the two vertical sides by rigid planes. The oscillations that arise are considered to be caused by simple shear on the assumption that the amount of distortion due to bending is very small.

The method assumes that the rigidity of the material is constant. This was considered appropriate in the case of GEM 1 and 2 as the levels of residual pore pressure were small . Only the primary mode of oscillation was considered. The calculation was carried out at prototype scale. For a scale factor N = 80 the equivalent input frequency is 1.5 Hz.

It is clear from Table 3 that the embankment natural frequency is considerably higher than the predominant driving frequency, and towards the upper end of earthquake frequencies observed in the field. This supports the finding of minimal amplification seen in the accelerometers and provides further indication that ACC 1932 has been incorrectly scaled in the data processing.

2.4 Phase differences

The phase difference between the base of the embankment and the other transducers was determined for the two tests by inspection from the recorded traces. A small phase shift may be expected due to the transmission time for the base input wave to reach the crest, depending on the stiffness of the soil, and provided the response remains stiff. Near resonance this phase shift will increase and at resonance ie. when the driving frequency is the same as the natural frequency, a phase lag of 90° should be observed. In some model tests, liquefaction has led to phase lags of nearly 180 ° in the fully softened condition.

In these model tests no significant phase differences between the base of the embankment and the rest of the soil were observed in any of the recorded traces, except for PPT 6159 in GEM 1. The lag of 180° at PPT 6159, which is on the downstream shoulder, was due to its location on the opposite side of the embankment to the other PPTs, as discussed above.

2.5 Mechanisms

The stability of both upstream and downstream slopes was investigated using the slope stability analysis program *Slope*[11]. The *Slope* program was used to provide a qualitative grasp of the likely failure mechanisms and to demonstrate the change in slope stability under

[11] DL Borin (1993), Slope - Slope stability and reinforced soil analysis program, Geosolve, Version 8.2.

quasi-static conditions of horizontal and vertical acceleration and the generation of excess pore pressures. Table 8 presents a summary of the findings for each of the embankments analysed. Appendix A describes the *Slope* calculation in more detail.

The GEM 1 experiment showed no evidence of deep-seated failure but profile measurements taken before and after indicated some crest settlement and heave of the slope on the side with the loose pocket. There may also have been some shallow superficial concoidal slips on the dense side of the embankment.

The absence of deep-seated failure may have been linked to the use of water as a pore fluid and the consequent lack of significant residual excess pore pressure at the end of the earthquake. Evidence from full scale events such as the 1939 Ojika earthquake and the 1971 San Fernando earthquake supports the finding that large scale slope movements require pore pressures to be maintained after the base shaking has ceased.[12] Most of the embankment dam failures in the Japanese earthquake occurred between a few hours or up to 24 hours after the seismic event. The San Fernando Lower Dam is reported to have failed some twenty minutes after the earthquake as high excess pore pressures were redistributed within the embankment.

The *Slope* analysis of the GEM 1 embankment is broadly consistent with the experimental observations, indicating a near planar shallow slip surface with a minimum factor of safety (FS) of 1.0 (equally likely on either side of the embankment) under 12% lateral acceleration (with no vertical component), Table 8 and Figure 1.

The most likely mechanism may be:

1. Strong motion input causes densification of the whole embankment. This causes the crest to slump and localised surface slips to spread the crest. A bulge in the slope profile is formed on either shoulder.

2. The relatively large residual pore pressures in the loose pocket lead to preferential spreading towards the loose side.

3. The change in the pattern of excess pore pressure development at the base of the loose layer after earthquake 1 indicates a marked reduction in mean effective confining pressure after the first shaking event. This may be due to arching over some portion of the loose zone, leaving it in a lightly stressed condition under near zero static shear stress.

[12] Bolton Seed H, Makdisi FI, DeAlba P (1978), Performance of Earth Dams during Earthquakes, Proc ASCE, Journal of the Geotechnical Engineering Division, Vol 104, No GT7, pp 967-994.

4. Local, shallow surface slips occur on the dense side.

Despite the much higher amplitude of input earthquake in GEM 2 compared to GEM 1, the embankment still does not appear to break up into distinct blocks or zones, nor are the excess pore pressures sustained in the long term. Instead its behaviour is also dominated by densification and slumping. Such a response is most likely due to the cyclic variation of shear stress and absence of residual excess pore pressure; high residual excess pore pressures and large lateral accelerations would be expected to lead to sliding type mechanisms and deep seated failures, as observed in the later experiments (discussed below).

A *Slope* analysis was again undertaken to provide a qualitative grasp of the stability of the embankment under lateral acceleration. In the *Slope* calculation the pore pressures in the loose zone were increased by 30 KPa (the maximum positive excess pore pressure generated in this zone) and the stability checked under conditions of 23% lateral acceleration. Table 8 and Figures 2 and 3 show that this produced highly unstable conditions on both sides of the embankment, with the loose pocket side being rather more critical.

As discussed above, the evidence from the accelerometer records for distinct episodes of downslope sliding is not present on the dense side, and there were no accelerometers on the loose side. Indeed, the symmetry of the "shark's teeth" response on the accelerometers is an indication of some global behaviour which is unrelated to the cycles of excess pore pressure in any local area and may instead be associated with the overall embankment response. It was explained above that the pore pressures on opposite sides of the embankment cycle out of phase, resulting in cycling stiffness and strength on alternate sides during each half cycle. Under these conditions, the embankment will cease to respond in a perfectly symmetrical manner (ie. response indistinguishable on loading and unloading, regardless of direction of acceleration) but will develop a 'mirror' symmetry on each half cycle as a function of the alternating high and low shear stiffness within each side of the embankment.

The factors of safety calculated using a combination of high excess pore pressure and high lateral acceleration are unsustainable in practice and in fact the absence of clearly observable slip surfaces suggests that this particular combination may not be strictly valid. Furthermore, the membrane may have had some unquantifiable influence in preventing deep seated failure on the loose pocket side. Nevertheless, the most likely cause for the limited movements in GEM 2 remains the rapid drainage which reduces the potential for sustaining residual pore pressures during shearing.

The mechanism of deformation for GEM 2 was therefore dominated by densification and lateral spreading, much as with GEM 1, possibly accompanied by some shallow movements on one or both slopes.

3. ENCAPSULATION OF LOOSE ZONES

As with GEM 1 and GEM 2 two grades of sand were used in the four models GEM 3, GEM 4, GEM 5 and GEM 6: Leighton Buzzard 52/100 medium dense sand for the dense section of the embankment and a fine grained Nevada sand for the loose pocket or zone. Details of these sands were given in Section 2.0 above. All four of the models used silicon oil as a pore fluid, with a viscosity of 80 cS, such that the time scales for diffusion and inertial effects were identical. The general layouts and locations of the pore pressure transducers and accelerometers in these four experiments are given in the 1992 data report. Because of the significant differences in model geometry, the experiments are discussed in order below.

3.1 Wide, shallow loose zone

In model GEM 3 the zone of relatively loose Nevada sand formed a wide and shallow region towards the upstream toe of the embankment. The loose layer was 'capped' with relatively impermeable water-saturated sheets of lasagne, simulating a thin layer of clay or other impermeable boundary in the field. Drainage laterally was restricted by the use of vertical latex rubber sheets on each side of the loose zone. Two pore pressure transducers and one accelerometer were located in the loose zone. All four input accelerations were of approximately similar magnitude. The mean peak input accelerations were 17% g, 18% g, 20% g and 21% g.

3.1.1 Development of excess pore pressures

Pore pressure transducer PPT 5409 shows a rapid build up of positive excess pore pressures in the relatively loose Nevada sand. This behaviour is recorded in all four earthquakes. The time histories of both PPTs in the loose zone, PPT 5409 nearer the core and PPT 3139 nearer the toe of the embankment show that the positive excess pore pressures were maintained beyond the end of the strong motion input as expected from the use of the more viscous pore fluid. From the middle of earthquake 1 onwards it is apparent that PPT 5409 is achieving the maximum possible excess pore pressure at around 46 KPa, indicating initial liquefaction. Comparison with the accelerometer in the zone above the loose pocket, ACC 3492, shows that the periods of liquefaction coincide exactly with periods of downslope slippage. The other pore pressure transducer in the loose zone (PPT 3139 towards the toe of the embankment) shows a more pronounced cyclic behaviour with positive and negative excess pore pressures. There is also an increasing tendency for a net positive

excess pore pressure to remain after the end of each strong motion input. This behaviour is most marked in earthquake 4. There is no tendency towards flattening of the positive peaks, but the pore pressures are in phase with PPT 5409, with the maxima corresponding to periods of downslope movement. The contrast between PPT 3139 and PPT 5409 may indicate that despite the impermeable boundaries around the loose zone, drainage was possible near the toe.

There were three pore pressure transducers in the relatively dense Leighton Buzzard sand forming the central section or core of the embankment. These were at the crest, at mid-height and at the bottom. Baseline fluctations in PPT 6260 (at the crest) appear to have distorted the data recorded particularly during earthquakes 1 and 2, but this effect is greatly diminished in earthquakes 3 and 4. The saw tooth nature of the positive excess pore pressures cycles may be caused by a combination of liquefaction and movement occuring simultaneously.

It is possible that the negative residual pore pressures evident after earthquakes 1 and 2 are indicative of shearing, but this seems unlikely as there is no evidence of sliding movement continuing after earthquake 1 and possibly not after earthquake 2. Downslope sliding is evident at ACC 3492 during earthquake 1 with a threshold of around 8%g; in earthquake 2 sliding occurs both ways during shaking with marked thresholds at ACC 3492 and at ACC 5701 on the dense side. (The large values of acceleration recorded at ACC 5701 should be treated with caution.) However, at the end of shaking both transducers broadly follow the base motion without indication of further movement. Evidence of post-earthquake movement is discussed further below.

PPT 6264 in the middle of the core shows strongly alternating positive and negative pressures with some residual excess pore pressure after the strong motion input is ended. The positive peaks are clearly flattened in earthquakes 2 through 4, indicating initial liquefaction (at around 20 KPa). At the base of the central core (PPT 6261) generation of large positive excess pore pressures which is maintained beyond the strong motion input is observed during all earthquakes. Again, in later earthquakes the positive peaks tend to become flattened and the negative peaks become very sharp, indicating brief periods of liquefaction (at around 48 KPa). This is quite significant as the transducer is near the base of the core of the embankment, in the dense material. Its peak positive excess pore pressures coincide with the peak pore pressures on the loose side of the embankment.

Above the loose zone around mid-slope PPT 6269 shows large positive peak excess pore pressures, which drop steadily as movement takes place (as indicated by sliding at the adjacent accelerometer ACC 3492) and then fall rapidly on reversal of loading, in phase with the PPTs in

the loose zone (PPTs 5409 and 3139), giving a bi-linear effect. Positive recovery from peak negative values is likewise bi-linear with a steady (but rapid) rise through one quarter cycle and then a near instantaneous leap to the peak positive value through the next quarter cycle.

At the toe PPT 6514 shows some significant peak positive excess pore pressures in earthquake 1 but no residual pore pressure. By earthquake 3 (and particularly in earthquake 4) small residual negative excess pore pressures are generated which persist after the earthquake for over 60 milliseconds, further evidence of continued sliding movement after the shaking.

On the dense side of the embankment at mid-slope PPT 6270 is clearly very shallow but appears to show periods of fluidisation (initial liquefaction) at around 4 KPa with sharp negative pore pressure cycles on reversal of loading (coincident with maximum positive pore pressures on the opposite side of the embankment). The nearest accelerometer mid-slope on the dense side, ACC 5701, shows very clear evidence of downslope sliding or slippage during the periods of high excess positive pore pressure. PPT 5407 was not reported.

3.1.2 Accelerations

The behaviour of the loose zone was recorded by accelerometer ACC 1926. In all four earthquakes, but most markedly in earthquakes 2, 3 and 4, ACC 1926 shows evidence of sliding or slip in one direction with a threshold of around 12%. As the periods of liquefaction in the loose zone become proportionately longer, and therefore the periods of positive effective stress become correspondingly shorter, the negative peaks of acceleration become progressively sharper and more strongly amplified, indicating the severity of the 'snatch' effect as the particles in the liquefied soil suddenly re-engage.

Interestingly, slip or sliding in the dense slope above the loose zone is triggered after movement has started in the loose zone below. In the case of earthquake 1, movement on the slope (indicated by ACC 3492) starts as movement in the loose zone has all but stopped. This indicates that there may be several mechanisms acting in the embankment response.

ACC 3492 also differs from ACC 1926 as it shows a extremely flat response once the threshold has been reached. By earthquake 4 this threshold appears to reduce with time, and the record shows clear evidence of continued sliding after shaking has stopped, for over 60 milliseconds in the case of earthquake 4. During the 'aftershock' cycles, which continue for around 40 milliseconds after the main shaking has stopped, the threshold at ACC 3492 falls to only a few percent of g.

The flat threshold acceleration is indicative of a very simple mechanism, such as a single block or planar slide. The more rounded response at ACC 1926 after the threshold is reached is indicative of a more complex kinematic mechanism, probably involving multiple block movement or non-planar movements.

In the core of the embankment the crest accelerometer ACC 3477 appears to show attenuation of the base acceleration in earthquake 1 in a pattern often characteristic of base isolation due to liquefaction in level ground, but it may in fact also be showing evidence of downslope movement linked to the response of the mid-slope accelerometer ACC 3492 below it. In the subsequent earthquakes this behaviour becomes more pronounced and the sliding mechanism which involves ACC 3492 clearly also involves the crest accelerometer, ACC 3477. Tables 9, 10, 11 and 12 present an analysis of amplification at selected accelerometers in earthquakes 1, 2, 3 and 4 respectively.

The response of ACC 1225 is difficult to interpret and the device may be unreliable. On the other hand in its central location in the embankment it may have been affected by several sliding mechanisms, possibly in both directions, and this may explain its unusual character. Careful examination of the individual data points and their correlation with other records would be necessary to reach any firm conclusions. The base accelerometer ACC 5754 did not record a trace due to amplifier failure.

ACC 5701 on the dense side of the embankment (mid-slope) also shows clear evidence of downslope movement during earthquakes 2, 3 and 4, but in a separate mechanism to the slip on the loose side. As noted above, the high values of acceleration raise questions over the magnitude of the accelerations, but qualitatively the data is valid. In earthquake 2, the response during movement starts 'flat' indicating a single block type movement, but this quickly becomes rounded, within a few cycles, indicating a more complex multi-block sliding mechanism. This rounded response post-threshold is characteristic of the behaviour during earthquakes 3 and 4 also.

It is clear, therefore, that translational failure occurred on both sides of the embankment. The more extensive failure which occurred over the loose zone incorporated the crest (ACC 3477) and the slope around ACC 3492. Spreading occurred at depth, evidenced in the loose zone (ACC 1926). The opposite dense side slope (ACC 5701) also shows downslope movement. Close examination of the timing of the movements suggests that, during each cycle, sliding is nearly continuous and in the following sequence:

1. movement is initiated in the loose zone;
2. shortly afterwards, movement starts on the loose side slope above;

3. movement stops in the loose zone, continuing on the slope above;
4. movement stops on the loose side slope and starts on the dense side;
5. movement stops on the dense side and starts in the loose zone again.

3.1.3 Phase and natural frequency

Examination of the phase difference between the base (ACC 3436 on the box as ACC 5754 at the base of the embankment was not available) and each of the other accelerometers was made for earthquake 1, which was considered more relevant than the later earthquakes because the scale of movements was less. Although at the start of shaking, during the first cycle, all accelerometers are roughly in phase, by the eighth cycle the crest of the embankment and mid-slopes on either side (ACCs 5701, 3477 and 3492) lag the core of the embankment (ACC 1225) and the base (ACC 1926) by nearly 180°, indicative of a resonant response.

Theoretical calculation of the natural frequency of the truncated wedge above each accelerometer was carried out with the given inputs following the Ambraseys method. This calculation shows resonance expected at ACC 5701 only, which had a natural frequency of 2.4 Hz in earthquake 1 dropping to around 1.5 Hz in earthquake 2 to earthquake 4. However, this neglected the effects of the excess pore pressure, which would be expected to show a marked decline in the natural frequency at other locations in the upper portion of the embankment also. It is therefore considered valid that the large phase lag observed in the upper accelerometers is indicative of a resonant or near resonant response in the embankment.

3.1.4 Mechanisms

Slope stability analysis of the embankment in GEM 3 did not yield a solution because the high excess pore pressures caused liquefaction leading to computational problems with the *Slope* program. A second attempt, using $R_u = 1.0$ in the loose zone instead of raised piezometric levels did not indicate failure, possibly due to the high strength elsewhere, Table 8 and Figures 4, 5 and 6.

However, as discussed above it is apparent that extensive movements took place in the GEM 3 experiment, both during the earthquake shaking and afterwards as movements continued for some considerable time. The profile of the embankment measured afterwards showed substantial settlement of the crest and spreading towards the loose side of the embankment in particular, with a concoidal slip zone on the loose side in the lower half of the slope. Settlements were greatest over the central two thirds of the length of the embankment, suggesting some three dimensional effects or restraint towards each end, against the walls of the strongbox.

Although the sequence of movement can be determined quite precisely from the accelerometer records (described above), exactly which mechanism was triggered first is more difficult to deduce. From earthquake 2, in which all three mechanisms are invoked, it is clear that the slope above the loose zone starts to slide by the onset of the second positive peak of shaking. ACC 3477 at the crest above appears to respond through this cycle, but as soon as the slope below slides on the third positive peak, it follows and thereafter mirrors the movement on the slope below. On the dense side of the embankment, movement occurs on the opposite phase but it would appear that the dense side starts to slide on the second negative peak (between the second and third positive peaks). Movement in the loose zone itself is may not have been initiated until the fourth or fifth positive peak of acceleration.

The embankment then breaks up in the following sequence:

1. part of the loose side slope slides under a combination of high excess pore pressure and acceleration;
2. the dense side slope moves almost immediately afterwards;
3. the crest moves, following the loose side;
4. deeper mechanisms reach the loose zone and spread the embankment laterally; once invoked, movement occurs here before it is triggered on the slope above;
5. the initial planar slide on the dense side involves more blocks; its threshold falls;
6. the threshold for the loose side slope movement falls to half its initial value; movement continues on the loose side for some time after the end of shaking.

In the third and fourth earthquakes of the sequence, all mechanisms are triggered on the first significant cycle.

3.2 Deeper loose zone

In experiment GEM 4 the zone of relatively loose Nevada sand on one side of the embankment was deeper (40 mm instead of 30 mm), but less wide (135 mm instead of 175 mm) and was positioned closer to the core than in GEM 3. Otherwise its construction, using latex rubber sheets at either side of the loose zone and water saturated sheets of lasagne to form a low strength impermeable layer on top, was identical to GEM 3. Two pore pressure transducers and one accelerometer were located in the loose zone. The four earthquake events had input accelerations which gradually increased in magnitude. Mean peak input accelerations were 15% g, 21% g, 23% g and 27% g, respectively.

3.2.1 Development of excess pore pressure

In the loose zone near the core the rapid build up of positive excess pore pressure is shown by PPT 6261 in all four earthquakes. The retention of positive excess pore pressure is even more effective than in GEM 3, as pore pressures near 100% are sustained (at around 20 KPa) for most of the period of shaking, without interruption. Although clearly indicative of liquefaction, this absolute value is much lower than expected for its location in the embankment.

PPT 3139, also in the loose zone but closer to the toe, shows liquefaction at around 25 KPa, a value consistent with its location. On the other side of PPT 6161, PPT 5409 at the base of the core of the embankment also reaches initial liquefaction (at around 56 KPa) although at a similar depth to PPT 6261. (PPT 5409 also shows double frequency cycling, characteristic of both very low static shear stress and very low effective confining pressure.) It is concluded that the numerical values indicated by PPT 6261 are in error, although the data is qualitatively valid.

The long term record (from earthquake 4) further shows the effectiveness of the impermeable boundaries to the loose zone. The high excess pore pressures are clearly sustained in the loose zone for many seconds, equivalent to many minutes in the field.

Above the loose zone, around mid-slope, PPT 6514 shows liquefaction (at around 10 KPa) with sharp negative pulses on reversal of loading. This pattern is consistent throughout the four events with rapid drainage after the end of shaking. At the toe on the loose side PPT 6270 shows a positive residual excess pore pressure but with a strong cyclic character. The amplitude of the cycles builds up over the four earthquakes with the peak positive value remaining roughly constant at around 12 KPa (neglecting noise). The increase in amplitude of the cycles is not directly related to the increasing amplitude of the base input and hence is indicative of a steadily reducing effective confining pressure after each earthquake, with the static shear stress maintained.

In the centre of the embankment at the crest PPT 3000 initially shows the generation of net positive excess pore pressures but before the end of earthquake 1 this has become a net negative pressure. Net negative excess pore pressures are also developed in earthquake 2, but in the two remaining earthquakes the trace becomes more symmetric. In earthquakes 3 and 4 the traces seem to indicate a double frequency response. It is possible that after the first earthquake this device is extremely close to the surface, and perhaps in a fluid filled void.

PPT 6269 suffers from some electrical interference in earthquakes 2 and 4 but shows clearly a near liquefied condition (at around 27 KPa),

particularly during earthquakes 3 and 4. These are sustained beyond the end of shaking due to the long drainage path from this region.

At the base of the core PPT 5409 (already mentioned above) also indicates the strong generation of positive excess pore pressures and a condition of initial liquefaction but with a marked double frequency 'butterfly' response indicative of cycling shear stress in the presence of a very low effective confining pressure.

Two transducers recorded the behaviour of the soil on the dense side of the embankment. At mid-slope PPT 6260 shows the generation of net positive excess pore pressure with initial liquefaction at around 12 KPa with a relatively high residual positive excess pore pressure The periods of liquefaction are terminated abruptly with near instantaneous falls in pore pressure exactly coincident with interruptions to the downslope movement under reversal of loading (shown by the adjacent accelerometer ACC 1932).

At the toe on the dense side PPT 6264 shows the generation of small cyclic positive and negative excess pore pressures with a very slight net positive excess which is not sustained in the long term. The maximum mean positive excess pore pressure is around 4 KPa and may be indicative of initial liquefaction, but the PPT is very shallow and there is significant noise overlying the small signal. Its behaviour is quite consistent over the four events.

3.2.2 Accelerations

In the loose zone, ACC 3492 shows a response very similar to ACC 1926 in the same location in GEM 3, with evidence of lateral movement developing in the larger, later earthquake events. In earthquake 1 a bi-linear response develops during each half cycle, but peak accelerations are sustained as high as -16% g. However, in earthquake 2 and particularly in earthquake 3 and 4 a clear threshold is seen, initially at around -12% g, dropping with successive cycles towards the end of the shaking to -9% or less. There is no evidence at this device for movement continuing after the earthquake.

On the same side of the embankment but above the loose zone ACC 1926 shows a highly asymmetric trace developing from midway through earthquake 1 with flat negative peaks and a sharp positive peak. Although the signal suffers from electrical interference in the remaining earthquakes, some qualitative information can be seen intermittently. It is clear that substantial movement took place in this part of the embankment.

In the centre of the embankment at the crest ACC 5701 shows an initially symmetric reponse which quickly deteriorates in favour of

movement towards the loose side with large positive peaks and rounded negative peaks. The strongly rounded nature of the negative cycles indicates that movement was complex, probably involving settlement and lateral movement. Similar behaviour is observed at mid-height in the core (ACC 3441) which shows the development of a relatively sharp threshold in the negative sense from earthquake 2 onwards. In earthquake 1, ACC 3441 does not show any evidence of movement until the fourth or fifth cycle, and even this is not particularly clear.

In contrast to GEM 3, in GEM 4 data was captured from an accelerometer at the base of the embankment in the core, ACC 3447, which showed a strongly symmetric behaviour, with accentuated peaks in both positive and negative directions of acceleration. These sharp peaks coincide exactly with the peak positive pore pressures at the adjacent pore pressure transducer, PPT 5409, which shows a response at twice the main driving frequency (as noted above).

ACC 1932 on the dense slope also shows marked evidence of downslope movement which develops strongly during earthquake 2 and later events. The strongly rounded nature of the acceleration on the negative cycles suggests a complex mechanism, with movement occuring out of phase with the movement on the loose side and in the core of the embankment. There is some overlap with movement in the core, however, and this may have affected the response at ACC 3441. As with GEM 3, the absolute values of acceleration for this device should be treated with caution, as they seem unreasonably high. The signal should have been inverted during processing to be consistent with the other devices (polarity of the device depends on its orientation in use).

Evidence of first movement in GEM 4 is therefore seen on the slope above the loose zone, as in GEM 3. ACC 1926 shows a rounding of the peak accelerations with the first cycles of earthquake 1, as soon as the excess pore pressures at the adjacent PPT 6514 have reached the full overburden. As this develops over the next few cycles into a downslope movement there is some evidence of spreading reaching the loose zone itself, at ACC 3477, although this is more pronounced in later events and in the core (ACC 3441). The initial 'loosening' of the upper part of the embankment shows itself at the crest as a symmetrical shark's tooth behaviour, which then follows the down slope trend towards the loose side (ACC 5701). On the dense side there is little evidence of movement in earthquake 1, but in the following events this becomes more pronounced. Tables 13, 14, 15 and 16 present an analysis of amplification at selected accelerometers in earthquakes 1, 2, 3 and 4 respectively.

3.2.3 Phase and natural frequency

An examination of the phase difference between the base accelerometer (ACC 3477) and the other accelerometers in the embankment shows that ACC 5701 at the crest lags the base by between 90° in earthquake 1 and over 120° in the later earthquakes 2 to 4.

The natural frequency for the embankment based on ACC 5701 was calculated as 2.9 Hz for earthquake 1 suggesting that the upper part of the embankment has a natural frequency low enough to be near resonance during the four earthquakes in the GEM 4 experiment.

Calculations incorporating the effects of excess pore pressure also showed that the natural frequency at ACC 3441 in the core was reduced from 7.0 Hz to 4.7 Hz, and at ACC 3492 in the loose zone from 13.1 Hz to 10.8 Hz by earthquake 4. ACC 3441 shows some phase lag whereas ACC 3492 remains closely in phase with the base input despite the high excess pore pressures in the loose zone.

3.2.4 Mechanism

The increase in input acceleration from earthquake 1 to earthquake 2 caused mechanisms which had been triggered in earthquake 1 to be extended and new mechanisms on the dense side to be invoked. In earthquake 2 and later events, movements become widely distributed throughout the structure, with the dense side slope also showing combined settlement and translation.

The character of the mechanisms, and the resulting profile, is similar to GEM 3 providing further confidence in the results. Again, no single slide or mechanism is responsible for the gross deformations. Rather, a series of mechanisms involving shallow slope failure, sliding, spreading at depth and general settlement appear to have taken place. It is clear that under conditions of high excess pore pressure, removal of support for parts of the embankment by one mechanism will inevitably lead to other movements.

As with GEM 3, a sequence of movements can be determined within the embankment GEM 4:

1. lateral spreading is initiated in the loose zone; pore pressures near the toe of the loose zone are rising sharply, and continue to rise but at a slower rate;
2. shortly afterwards, movement commences on the slope above the loose zone, in the core and at the crest; pore pressures nearby in the slope are at a maximum level (initial liquefaction); at the same time, movement on the dense side stops (movement on the dense side is

most clearly defined by the periods of peak pore pressure at the adjacent pore pressure transducer);
3. spreading in the loose zone then stops as the base acceleration has now reversed direction (becoming positive);
4. slightly later (due to phase lag), movement on the slope, in the core and at the crest stops; pore pressures on the slope start to fall rapidly from their maximum level; accelerations on the crest are rising rapidly (positive); at the same time, movement on the dense side starts again;
5. as the base acceleration reverses again, pore pressures in the loose zone reach a minimum and start to rise; accelerations in the loose zone increase and while movement continues on the dense side above, lateral spreading is again initiated in the loose zone.

Slope stability analysis using *Slope* was carried out both without allowance for excess pore pressure and with a range of values of R_u. Table 8 shows that under 23% g horizontally and 5% g vertically shallow slides are likely on both sides of the embankment, even in the absence of excess pore pressure. As excess pore pressures develop, the calculation shows that deeper mechanisms are invoked. This is probably due to the effect of the additional pore pressures in the soil near the top of the embankment on the restoring moment, which pushes the solution deeper. Examination of the predicted critical surfaces in Figures 7 and 8 shows how problematical such calculations are for predicting embankment performance in such a case.

3.3 Loose toe section

In this experiment a large section of the upstream toe of the embankment (250 mm from the toe towards the core) was formed from the relatively loose Nevada sand. A latex rubber membrane was placed vertically on the core side of the loose pocket to inhibit lateral drainage. Four pore pressure transducers and two accelerometers were placed in the loose zone. The mean peak amplitude of the input accelerations for the four earthquakes in the GEM 5 series was 17% g, 23% g, 26% g and 27% g respectively.

3.3.1 Development of excess pore pressures

Excess pore pressures in the core of the embankment and in the loose zone rapidly reached levels indicating initial liquefaction in earthquake 1, with the pattern being repeated in following earthquakes. At the base of the loose zone, PPT 3139 shows a mean maximum level of around 30 KPa with some cycling, particularly in the second half of the shaking. In earthquakes 2, 3 and 4, the maximum pore pressure reaches a slightly higher level, at around 39 - 40 KPa, probably indicative of deeper burial of the device. In these events, the flat peak values are sharply interrupted by negative pulses, with a rapid drop in pore

pressure followed by a steady rise back to peak. The drop coincides with the end of movement in the loose zone, and is shown also in PPT 5409, nearer the surface of the slope in the loose zone, and at PPT 6261, near the toe of the loose zone. PPT 5409 shows a fully fluidised level of around 15 - 17 KPa, with a generally high residual level. In the toe of the loose zone, PPT 6261 shows some evidence of a maximum excess pore pressure level of around 7 KPa, but with large cycles and evidence of dilation towards the end of earthquakes 2, 3 and 4 (most noticeable in the long term records), indicating shearing particularly during the second half of each event.

The change in character mid-way through an earthquake is most obvious in earthquake 2 where PPT 6260 on the slope on the loose side but above the loose zone, reaches a peak level in the first few cycles and then starts to exhibit dilation as down-slope movement in the loose zone below causes shearing in the embankment above. After the movement finishes, pore pressure redistribution from the core of the embankment causes a rise in residual pressure before an ultimate decay in the long term. In earthquakes 1 and 2, this behaviour is complemented by the nearby PPT in the top of the loose zone, PPT 6264, which shows an increase in excess pore pressure to a near maximum level as soon as the downslope movement commences.

Three transducers recorded the pore pressures in the core of the embankment. At the crest PPT 6265 shows the build up of small positive excess pore pressures in the early cycles of earthquake 1 followed by some cycling and dilation. In later events the data from this device becomes difficult to interpret due to the small signals.

PPT 6514 in the middle of the embankment shows the generation of large residual positive excess pore pressures which are sustained into the long term. Liquefaction is observed at a level of around 40 KPa with little cycling in earthquake 1, but more pronounced cycling in the subsequent events. Below PPT 6514, PPT 3000 was located near the base of the embankment. It too showed full excess pore pressure and initial liquefaction but at a level of around 60 KPa (see earthquake 2). Some cycling was observed during the latter half of earthquake 1 but in the subsequent events PPT 3000 showed a near constant maximum level interrupted by sharp negative pulses which had become quite pronounced by earthquake 4.

On the dense side of the embankment, PPT 6269 shows an unusual type of response that may be due to impact or other electrical problems. Its data is discounted. Likewise PPT 6270, in the toe of the dense side of the embankment, did not function.

The pore pressure data indicates that in the main section of the embankment, both in the dense core and in the loose zone, liquefaction

dominated the response, with maximum values of excess pore pressure being reached within the first two cycles of earthquake 1. Excess pore pressures were sustained for some time after the shaking had ceased, and redistribution led to very high pore pressures being maintained near the surface of the slope (eg. at PPTs 5409 and 6260) for a considerable period afterwards. Consolidation after shaking occurred most rapidly in the deepest location (PPT 3000) and at intermediate rates at PPT 3139 in the loose zone and at PPT 6514 at mid-height in the core.

The onset of cycling in the pore pressure records during earthquake 1 may be coincident with the triggering of downslope movements on the dense side. In subsequent earthquakes, peaks in pore pressure response throughout the core and the loose side coincide with periods of downslope movement. Sharp falls in excess pore pressure are coincident with reversal of acceleration and periods of downslope movement on the dense side (discussed below). There is no evidence from the pore pressure transducers of continued movement after shaking.

3.3.2 Accelerations

At the base of the loose zone ACC 3477 records a symmetric signal through each of the four events, with only slight evidence of lateral movement. There is some attenuation of the signal possibly linked to some flattening of the negative peaks in the latter half of earthquakes 3 and 4.

Also in the loose zone but closer to the surface, the trace recorded by ACC 3492 is broadly symmetric for earthquake 1 but becomes increasingly asymmetric in earthquake 2 with a threshold at around 12%. In earthquake 1, there is some attenuation of the base input motion, but this may be associated with the low pass filtering of the higher frequencies which has resulted in an unusually 'smooth' history. This behaviour is probably linked to the observation (see above) of 'smooth' cycling in the latter half of the earthquake in the pore pressure records at PPTs 5409 (adjacent), 3139 and 3000 (in the denser core).

(There are two different types of cyclic response at a PPT recording near maximum excess pore pressure: the first is a smooth cycling such as seen here at PPT 5409 in earthquake 1, probably associated with changes in mean effective confining pressure; the second is a flat response, interrupted by sharp negative pulses such as at PPT 5409 in earthquakes 2, 3 and 4, probably associated with changes in shear stress.)

The rounded negative peaks at ACC 3492 from earthquake 2 onwards are indicative of a complex mechanism of settlement and lateral movement. This behaviour becomes more pronounced in earthquakes 3 and 4. The response at ACC 3492 is the principal evidence for the spreading of the loose zone in GEM 5, particularly in earthquakes 2, 3 and 4. Despite the high levels of excess pore pressure in earthquake 1, this does not seem to have been associated with significant downslope movement on the loose side.

All the remaining accelerometers are in the dense zone. At the embankment crest ACC 3441 shows significant attenuation of the base input motion even during earthquake 1, probably due to the extensive liquefaction in the core of the embankment, with the average magnitude of the peak transmitted acceleration only 30% that of the base input motion. In earthquakes 2 and 3 there is a tendency to flat negative peaks and sharp positive peaks indicating some lateral movement but in earthquake 4 its response shows near total isolation after the first cycle as liquefaction occurs throughout the embankment. This is the first clear evidence of isolation of the crest of the embankment in the GEM experiment series. No information can be gathered from ACC 1932, at mid-height in the core, as electrical problems caused a loss of signal. Tables 17, 18, 19 and 20 present an analysis of amplification at selected accelerometers during earthquakes 1, 2, 3 and 4 respectively.

At the base of the embankment core ACC 5701 shows a broadly symmetric trace, similar to ACC 3477 in the loose zone, but with slight rounding of the negative peaks even in earthquake 1, indicating lateral movement towards the loose zone. This becomes more pronounced during earthquake 2 but reverts to a symmetric, if distorted, cyclic signal during earthquakes 3 and particularly 4. The reason for the distorted signal is not clear.

The only accelerometer on the dense side, ACC 1572 at mid-slope, shows a marked asymmetry in the trace it records, indicating down-slope movement. During earthquake 1 the signal shows a baseline drift but this corrects itself in earthquake 2, which shows perhaps the clearest indication of a initially flat threshold for downslope sliding, gradually reducing and becoming more rounded as the earthquake progresses. By earthquake 3 and earthquake 4 this signal has become extremely distorted, with unrealistic negative pulses interrupting a generally 'flat' response. The interpretation of this extreme signal is not clear.

3.3.3 Phase and natural frequency

An examination of the phase difference between the base of the embankment and the other accelerometer locations showed ACC 1572

on the dense side slope of the embankment lagging the base motion by around 60°, 90°, 90° and 90° in the four earthquakes. ACC 3492 on the slope of the loose zone was the only other accelerometer to show a significant phase difference (around 60°, 60° and 90° in earthquakes 1 to 3).

Calculations following the Ambraseys method predicted resonance of the embankment based on ACC 1572 in all four tests. The natural frequency calculated using ACC 3492 varied from 6.1 Hz to 4.1 Hz over the four earthquakes.

A revised calculation was carried out incorporating the effect of the excess pore pressure generated as a result of the strong motion input. The revised calculation showed that for ACC 3492 in earthquakes 1, 3 and 4 the excess pore pressure generated was sufficient to exceed the initial vertical stress making further analysis invalid. For earthquake 2, a natural frequency of 0.8 Hz was calculated, suggesting a very 'flexible' response.

With the revised method the natural frequency at ACC 3441 (the crest accelerometer) was 2.4 Hz in earthquake 3 and 2.8 Hz in earthquake 4 so again there is a close coincidence of driving frequency with natural frequency.

3.3.4 Mechanism

One of the several unusual features of this experiment was the complete isolation of the crest, with accelerations here only 30% of the base input in earthquake 1, and near zero in earthquake 4 for most of the event. Translational sliding failure on the loose side is not obvious (at ACC 3492) until earthquake 2 when the relatively loose zone of Nevada sand at the upstream toe became unstable under the combination of lateral acceleration, high excess pore pressure and driving force from the core of the embankment above. The progressive 'hardening' in the response of PPT 5409, which is located under the slope in the loose zone probably indicates densification, but the surface of the slope continues to be fluidised on each earthquake by pore pressures from below. ACC 3492 shows the eventual sliding failure in earthquake 2. This zone of movement then deepens to encompass ACC 3477 in later events.

All the central and loose side accelerometers (including ACC 5701 at the base of the core of the embankment) show movement in the same direction in earthquakes 3 and 4, indicating a very large volume of the embankment is involved in the main translational mechanism. This was not seen in the earlier experiments, GEM 3 and GEM 4.

On the dense side of the embankment movement is seen at the shoulder (ACC 1572 and PPT 6269) from the beginning of earthquake 1. Large translational movements continued to occur in the following events.

Post-test measurements of the profile of GEM 5 indicated dramatic densification of the embankment with considerable loss of volume. The very high excess pore pressures generated at all locations appear to have liquefied practically the entire upper part of the embankment, leading to a large scale slumping and spreading, perhaps without any distinct slip mechanisms forming (except on the dense slope, which shows a similar type of response to the earlier experiments). The isolation of the embankment crest in earthquake 4 suggests that the main core had reached its final elevation after earthquake 3 and lateral movements which continued to be observed in ACC 3492 were probably associated with reshaping of the outer slope, towards the toe. The sequence of movement is difficult to determine, partly due to the location of the transducers, but it is postulated that movement took place in the following order:

1. very rapid development of excess pore pressures trigger shallow slides on the dense side of the embankment; the presence of the rubber membrane may have inhibited sliding on the loose side;
2. some movement on the loose side starts to take place in earthquake 1;
3. a large deep mechanism forms on the loose side during earthquake 2 as the loose zone spreads laterally, drawing the core of the embankment behind it; shallow sliding continues on the dense side;
4. movement towards the loose side continues during earthquake 3, still involving most of the embankment; shallow sliding continues on the dense side;
5. shallow sliding continues on the loose side in earthquake 4, but the core of the embankment is now settled and responds more as a one dimensional column with fluidisation of the upper portion but no lateral movement.

Examination of the GEM 5 geometry using the *Slope* program, Table 8 and Figures 9, 10 and 11, modelling both the excess pore pressures and an input earthquake similar in amplitude to those observed in these four tests suggested the possibility of a deep seated failure on the loose side of the embankment as described above.

3.4 Large loose zone extending to the toe

In the final model of the series, GEM 6, the zone of relatively loose Nevada sand was at the upstream toe of the embankment. This was similar to the wedge in GEM 5 but was truncated so that it was reduced in vertical extent. A vertical latex rubber sheet was placed on the side of the loose zone nearest to the core to restrict lateral drainage and

water saturated lasagne sheets formed a low strength impermeable boundary over the top of the loose zone. The data set from GEM 6 was probably the most consistent in terms of quality of the GEM experiment series and instrumentation problems appear to have been minor. There were four pore pressure transducers and one accelerometer in the loose zone. The four input accelerations varied considerably in amplitude with mean peak input accelerations of 12% g, 18% g, 21% g and 23% g.

3.4.1 Development of excess pore pressures

There were four pore pressure transducers in the loose zone of the embankment, all of which responded well during the shaking events. The primary response of the loose zone can be seen clearly in PPT 6261 and PPT 6265, which were furthest from the slope. Both PPTs show a steady rise in excess pore pressure, not reaching full overburden (initial liquefaction) until the fifth or sixth cycle of shaking in earthquake 1. In subsequent earthquakes, the peak positive excess pore pressures were reached within the first couple of cycles of shaking. PPT 6261 reached a maximum excess pore pressure of around 45 KPa (neglecting noise) and PPT 6265 reached about 28 KPa. Long term records show these pore pressures being sustained for a long period after the shaking, confirming that even though the loose pocket was 'open' where it met the slope, the impermeable boundaries on three sides of the zone were highly effective in restricting drainage.

With successive earthquakes, both PPTs indicate some 'hardening' of their cyclic response with sharper negative pulses interrupting the otherwise 'flat' maximum pore pressure levels. Although in the first cycles of shaking the amplitude of the pore pressure cycles were comparable at the two transducers, it is noteworthy that as the shaking continues, the amplitude of the cycles becomes relatively much larger at the higher pore pressure transducer, PPT 6265, than at PPT 6261. Nevertheless, these records show clearly that the loose zone in GEM 6 behaves very consistently throughout the four earthquakes, and is largely liquefied throughout and for some time after each episode of shaking.

PPT 3139 was located closest to the toe in the loose zone and showed considerable cyclic variation with only a minimal build-up of residual pore pressure. The amplitude of the cycles during each earthquake was exactly proportional to the amplitude of the base shaking recorded at ACC 3436 on the box. Peak to peak amplitude increases from around 12 KPa during earthquake 1 to around 22.5 KPa in earthquake 4, while the base acceleration increased from a mean peak amplitude of 12% in earthquake 1 to 22.6% in earthquake 4. There was no indication of a maximum excess pore pressure being reached during any of the earthquakes; by earthquake 4 no residual pore pressure after shaking

was apparent at all. Photographs of the toe of the embankment after the experiment showed that PPT 3139 had moved to the surface of the slope and this may explain the response during earthquakes 3 and 4 in particular.

At the toe on the dense side of the embankment PPT 6264 showed a response very similar to PPT 3139, with strong cyclic behaviour and minimal residual pore pressure. The amplitude of the cycles at PPT 6264 is also very similar to PPT 3139 and closely related to the amplitude of the base shaking in each earthquake. It is likely that this PPT was also close to the surface of the slope.

Further up the slope PPT 5409 showed less cyclic variation but much higher residual pore pressure and by earthquake 3 and 4, clear indication of initial liquefaction (at around 9 KPa). During earthquakes 1 and 2 peak pore pressures also reached around 9 to 10 KPa, but only momentarily. During earthquakes 3 and 4 the response 'hardens' as the flat tops become more pronounced and the residual pore pressure is sustained for a considerable period after the earthquake, reflecting the slow drainage from the largely encapsulated loose zone.

Above the loose zone, but in the dense shoulder of the embankment PPT 3000 shows strong cyclic variations with large negative excess pore pressures reaching less than -30 KPa during earthquake 4. Maximum positive pore pressures of around 11 KPa indicating initial liquefaction are reached by the fifth cycle in earthquake 1, by the third cycle in earthquake 2 and on the first cycle in earthquakes 3 and 4. PPT 3000 showed negligible residual pore pressure after shaking. The onset of liquefaction coincided with downslope sliding as shown by the adjacent accelerometer, ACC 1900, and by the crest accelerometer ACC 3466 and this is discussed further below. Downslope movement continues after the main shaking in earthquake 4, where re-liquefaction on 'aftershock' cycles clearly triggered further downslope movement.

In the central section of the embankment three pore pressure transducers at different elevations showed a variety of responses. At the highest elevation, near the crest, PPT 6513 showed very high negative excess pore pressures in all four tests, with positive excess pore pressures reaching levels indicative of initial liquefaction by around the fifth cycle of earthquake 1 and thereafter within the first cycle of each earthquake. During the latter half of earthquake 1 a negative baseline drift overlays the record, and this occurs in all three successive earthquakes. The onset of the baseline drift is coincident with the onset of downslope sliding on the loose side, identified above at PPT 3000. Such behaviour is often indicative of dilation on shearing but in this case, within the overall negative impulse, flat tops are seen indicating initial liquefaction on successive cycles. After shaking, the residual negative pore pressure at PPT 6513 dissipates at a rate similar

to other transducers on the dense side. This slow dissipation suggests that the negative impulse is a real phenomenon, associated with the down-slope movement.

However, the reason for the negative impulse is not obvious. It is clearly associated with the crest of the embankment, as in earlier experiments similar behaviour is also seen at PPTs in a similar location. The large negative pulses, which appear to develop a negative residual excess pore pressure over a number of cycles, do not coincide with periods of movement. On the contrary, downslope movement towards the loose side coincides with the flat tops to the pore pressure cycles. For these flat tops to indicate initial liquefaction it is clear that the overburden pressure must be reducing, progressively, as if the soil was settling away from the transducer. After the earthquake, as the volume of fluid remains constant, there should be no permanent residual pore pressure unless the elevation of the PPT has changed. This explanation appears to fit most of the observations. However, it does not explain why the absolute level of pore pressure at which initial liquefaction takes place should be less than the final, drained, condition if the elevation of the transducer has remained constant.

From the long term records (for example earthquake 4) it is clear that there is no permanent shift or residual change in the absolute level of pore pressure at PPT 6513. Therefore there can have been no significant change in elevation of the device (10 mm settlement would correspond to a positive residual pore pressure of around 8 KPa). Given the extent of settlement and slumping of the crest which was observed it is concluded that the negative impulse must be associated with interaction between the PPT and the surrounding soil, and should therefore be treated with caution.

At mid-height in the embankment PPT 6269 showed a strongly cyclic response, with minimal residual pore pressure (some residual in earthquakes 3 and 4). During earthquakes 1 and 2, this PPT showed a symmetric 'steady' response. During earthquake 3, however, the record becomes unsymmetric with the amplitude of the positive peaks less than expected and during earthquake 4, a sudden increase in cyclic response is seen, combined with some higher frequency distortion on the positive side. This behaviour is quite different to earlier experiments (for example GEM 5) and suggests that in this case the core of the embankment was not able to densify further, and thus did not generate excess pore pressures, but retained its strength throughout the four events. It is interesting to note that the peak to peak amplitude of the pore pressure cycles are relatively consistent with earlier experiments in a similar location.

At the base of the central section PPT 6260 shows the generation of very high positive excess pore pressures during the strong motion input

with a significant positive residual pore pressure which drains in the long term over a period consistent with the other PPTs in the dense sand. PPT 6260 generates its maximum positive excess pore pressure during the first earthquake with a peak value possibly indicative of initial liquefaction at around 50 KPa towards the end of the shaking. This clearly acts to densify the sand in this zone, and in following earthquakes, although the peak positive residual is reached early, the absolute value is reduced compared to earthquake 1. At the same time, the amplitude of the pore pressure cycles builds up over the four earthquakes, and during earthquakes 3 and 4 reached a peak to peak value of around 32 KPa.

On the dense side slope PPT 6514 showed a very consistent response over the four earthquakes, with a steady rise of excess pore pressure during earthquake 1, reaching a peak positive value indicative of initial liquefaction (at around 10.5 KPa) by the fifth or sixth cycle, and a more rapid rise to a maximum value in following events. Also during earthquake 2 a double frequency response starts to develop, and during earthquakes 3 and 4 relatively sharp negative pulses of short duration become progressively more dominant in the response. The sharp negative 'spikes' correspond to similar sharp negative pulses in the nearby accelerometer ACC 3441, indicating periods where movement has temporarily stopped. As these spikes become more prominent, so the double frequency response becomes more unsymmetric, with a larger first peak than second, and the second peak gradually becoming overtaken by the sharp negative pulse or spike associated with the arresting of down-slope movement.

3.4.2 Accelerations

In the loose zone ACC 3492 showed a largely symmetric response in earthquake 1, with evidence of lateral movement towards the toe starting around the seventh negative acceleration cycle, at a threshold of around 10% g. In earthquakes 2, 3 and 4, there is clear evidence of lateral movement, and the nature of the cut-off becomes more rounded in earthquake 2, and then increasingly sharp, almost triangular in the latter half of earthquakes 3 and 4. The periods of lateral movement at ACC 3492 do not correlate closely with particular episodes of high or low pore pressure at the PPTs in the loose zone closest to the central section of the embankment, and coincides loosely with a period of rising pore pressure at PPT 5409, above the accelerometer in the loose zone. The movement correlates most closely with the negative half-cycle at PPT 3139 in the toe of the loose zone. This movement is therefore not considered to be the main mechanism on the loose side.

The main down-slope movement on the loose side of the embankment is shown by ACC 1900, above the loose zone, around mid-slope. In earthquake 1, ACC 1900 shows downslope movement being triggered

at a threshold of around 4 - 5% g on the fifth or sixth negative cycle (note the record should be inverted to show the same phase as the others). Thereafter, ACC 1900 shows downslope sliding (with relatively flat response after the threshold is exceeded) on all cycles in the following earthquakes, including the 'aftershock' cycles. It is therefore clear that movement continued downslope after the main shaking had ceased.

This downslope movement is also reflected clearly in the crest accelerometer, ACC 3466, which shows a rounded cut-off beyond a threshold of around 4 - 6% g. In the opposite sense, the acceleration pulses are sharp and highly amplified, with peak positive accelerations in excess of twice the base input (of the order of 30% g or greater). In this experiment there was also a vertical crest accelerometer, ACC 1572 which recorded in all earthquakes a response initially in phase and at the same frequency as the main shaking but which then exhibits a higher frequency response with some distinct pulses at constant time intervals, probably related to the starting and stopping of sliding movements. In earthquake 1, for example, ACC 1572 showed five sharp spikes during the latter half of shaking which appear to coincide with the end of slip on the dense side of the embankment. Whether this is significant, or even related, could be explored in future studies.

In the core of the embankment ACC 3477 and ACC 5701 (near the base) show generally symmetric response during earthquake 1, but during earthquake 2 and following events, the centre of the embankment at ACC 3477 shows evidence of significant lateral movement, with a clear threshold and the initially rounded response after the threshold is exceeded becoming increasingly sharp and triangular, with higher frequencies interfering in the underlying motion.

On the dense slope ACC 3441 showed clear evidence of downslope movement from mid-way through earthquake 1. In following events, the negative pulses became highly pronounced and showed extreme amplification, coinciding with the sudden development of positive effective stress and the 'snatching' of shear stress as the slope re-engages with the input motion. These snatched accelerations are also reflected in the pore pressure record at PPT 6514, nearby. The values of acceleration at ACC 3441 seem high and should be treated with caution. Tables 21, 22, 23 and 24 show an analysis of amplifications at selected accelerometers.

3.4.3 Phase and natural frequency

Examination of the phase difference between the base of the embankment and other accelerometer locations shows that the crest of the embankment (ACC 3466) has a phase lag of around 120° compared

to the base in all four earthquakes. ACCs 1900 and 3441 around mid-slope and ACC 3477 at mid-height in the central section also show phase lags of around 90°, indicating resonance in the upper portion of the embankment.

Calculations carried out following the Ambraseys method again showed natural frequencies comparable to the driving frequencies, both with and without the inclusion of excess pore pressures.

Resonance of the embankment may then be concluded to have occurred in GEM 6 as with several of the earlier experiments. Resonance may help to explain some of the extreme responses which were observed at a few transducers, including to some extent GEM 6 but most obviously in GEM 5 as discussed above. However, resonance of the embankment is not resonance in the classical sense of an elastic structure. The state of the embankment changes dramatically through each cycle of shaking: sudden changes of stiffness occur (both hardening and softening) during cycles of loading effectively altering the geometry of the structure at least twice during each cycle as far as it relates to its dynamic response.

As liquefaction occurs on alternate sides of the embankment during alternate halves of each loading cycle, the embankment cannot be considered symmetric in terms of elastic stiffness. The leading slope (in the sense of the direction of the lateral acceleration field) will transmit the shear stress as high as it can, accelerating the embankment in one sense or the other. The trailing slope, on the other hand, has no strength or stiffness and is likely to be disconnected from the leading slope by a sliding surface or shear zone for at least part of the loading. This situation reverses twice during each cycle of base shaking as the loading direction reverses. A form of resonance can be observed by analogy with conventional elastic models, but it is clearly not appropriate to interpret this behaviour too rigidly within a traditional elastic model of dynamic response.

3.4.4 Mechanism

GEM 6 was the most successful of the GEM experiments in terms of data recovered. The steady rise in positive residual excess pore pressure during earthquake 1 brought about a slope failure on both sides of the embankment about mid-way through the event. During earthquake 1, the down-slope movement on the loose side included the crest of the embankment, but the mechanism moved deeper during earthquake 2, taking in also the central core of the embankment, where movement is shown at the accelerometer in phase with the positive cycles of excess pore pressure in the core, but not apparently linked to liquefaction in the core.

Under large lateral accelerations, the mechanism of movement on the loose side appears to have moved deep enough to encompass the base of the loose zone itself, which showed some evidence of lateral spreading, but at a higher threshold acceleration than the slope above. Once triggered, movement at the base of the loose layer started fractionally before movement on the slope above, due in part to the phase lag before motions reached the upper parts of the embankment.

On the dense side, shallow down-slope movement occurs in all four earthquakes.

A slope stability calculation using *Slope* was carried out with a quasi-static horizontal acceleration of 21% g and a vertical acceleration of 5% g, Table 8 and Figures 12 and 13. The analysis predicted shallow slides on both sides of the embankment, with the loose side being marginally more critical than the dense side. Again, as with the earlier examples, examination of the slip surfaces predicted by the *Slope* model demonstrates that such calculations provide no insight into the complex mechanisms of movement which take place in practice.

4. CONCLUSIONS

1. The early experiments which used water as a pore fluid showed substantial settlements and some lateral spreading (towards the loose side), despite rapid drainage of excess pore pressure after the events.

2. In the second series of experiments, the use of silicon oil as a viscous pore fluid fluid enabled large residual excess pore pressures to be maintained during, and for a considerable period after, the shaking and this contributed to the development of gross deformations, including the formation of deep-seated mechanisms, particularly affecting the loose side of the embankment.

3. The use of water saturated sheets of lasagne (pasta) was successful in confining the excess pore pressures generated in the loose zones without restricting the ability of the sand to undergo gross deformation.

4. The use of silicon rubber sheets (membranes) to provide vertical boundaries was successful in preventing lateral drainage but there is some evidence that these sheets interfered with the development of shear zones and slip surfaces. This risk should be considered carefully in future applications.

5. The experiments can be subdivided into two groups: GEM 1 and 2, and GEM 3 to 6, each of which showed different characteristics of

deformation.

6. The early experiments, GEM 1 and 2, which used water as a pore fluid, showed initial liquefaction at the peak of positive pore pressure cycles at several locations including the loose pocket and at the toes of the embankment. However, deformation was dominated by densification, settlement and spreading, with shallow slips on one or both of the embankment slopes.

7. The latter four experiments, which used silicon oil as a pore fluid, showed much deeper mechanisms of movement, with the embankment breaking up into discrete elements.

8. In the oil-saturated models, very high pore pressures were sustained in the (encapsulated) loose zones and gross movements took place towards the loose side, with shallow sliding also occurring on the dense side of the embankment in all cases. As the shaking progressed, the mechanism on the loose side typically moved deeper, leading to spreading at depth, in the loose zone itself. Movement often continued after the main shaking had ceased.

9. In their dynamic response, the four latter models all showed evidence of substantial phase lag between the upper parts of the embankment and the base input, indicating a marked loss of stiffness and behaviour typical of resonance in an elastic system. The pattern of shear stress transmission through alternate sides of the embankment within each cycle of shaking had an increasingly marked effect on the character of the pore pressure and acceleration response as more of the embankment was degraded.

10. Traditional slope stability analyses based on finding critical slip surfaces did not provide any useful insight into the detailed mechanisms of deformation other than confirming that slope movements were likely. The slope stability analyses were not reliable where excess pore pressures were included. The accuracy of the calculations was not adequate to be useful in design and clearly alternative approaches to assess slope stability under seismic loading are needed.

11. These experiments confirmed the important role of the centrifuge in geotechnical earthquake engineering where modelling of field structures requires the study of complex deformation mechanisms combined with the effects of high excess pore pressures, liquefaction and consolidation.

TABLES

GEM 1 earthquake 1

	$\Delta u/\sigma'_v$ peak	$\Delta u/\sigma'_v$ residual	depth (m)	σ'_v (KPa)	Δu peak (KPa)	Δu residual (estimated) (KPa)	elevation (m)
PPT 6560	0.39	0.21	4.7	43	17	9	5.0
PPT 3156	0.56	0.3	3.2	30	17	9	3.0
PPT 6518	0.32	0.26	5.1	47	15	12	2.0
PPT 6269	0.2	0.05	2.2	21	4	1	1.8

Table 1: Calculation of $\Delta u/\sigma'_v$ for peak and peak residual excess pore pressure

GEM 1 earthquake 1

	Peak +ve (%)	Peak -ve (%)	Amplification (+ve)	Amplification (-ve)	Comments
ACC 1572	+/- 7.6*		1.3	1.1	crest (use average of max and min)
ACC 5701	+/- 5.5*		0.9	0.8	dense side, mid-slope (use average of max and min)
ACC 3441	5.7	-3.3	0.8	0.7	toe, loose side (drifting signal)
ACC 1552	5.9	-6.7	1.0	1.0	ref: base of embankment
ACC 5754	7.0	-6.3	1.19	0.94	top, loose pocket
ACC 1932	10.0	-11.0	1.69	1.64	mid-height, core
ACC 3436	5.9	-5.4	1.0	0.81	base, dense side

* corrected value, based on mean of peak positive and peak negative values

Table 2: Peak accelerations, GEM 1 earthquake 1

GEM 1 earthquake 2	Peak +ve (%)	Peak -ve (%)	Amplification (+ve)	Amplification (-ve)	Comments
ACC 1572					na
ACC 5701	+/-7.0*		0.7	0.6	drifting signal, mean of max, and min
ACC 3441	10.2	-9.1	1.05	0.83	toe, loose side
ACC 1552	9.68	-11.0	1.0	1.0	ref: base of embankment
ACC 5754	10.7	-12.7	1.11	1.15	top, loose pocket
ACC 1932	+/-18.9*		2.0	1.7	mid-height, core (drifting signal)
ACC 3436	9.26	-9.48	0.96	0.86	base, dense side

* corrected value, based on mean of peak positive and peak negative values

Table 3: Peak accelerations, GEM 1 earthquake 2

GEM 1 earthquake 3	Peak +ve (%)	Peak -ve (%)	Amplification (+ve)	Amplification (-ve)	Comments
ACC 1572					na
ACC 5701	13.5	-6.46	1.17	0.49	dense side, mid-slope: low -ve value due to slip
ACC 3441	10.5	-12.5	0.91	0.95	toe, loose side (drifting signal)
ACC 1552	11.5	-13.1	1.0	1.0	ref: base of embankment
ACC 5754	10.1	-15.0	0.88	1.15	top, loose pocket
ACC 1932	+/-24.3*		2.1	1.9	mid-height, core (drifting signal)
ACC 3436	10.4	-10.7	0.9	0.82	base, dense side

* corrected value, based on mean of peak positive and peak negative values

Table 4: Peak accelerations, GEM 1 earthquake 3

GEM 2 earthquake 1	Peak +ve (%)	Peak -ve (%)	Amplification (+ve)	Amplification (-ve)	Comments
ACC 1932	not reliable	not reliable			dense side, mid-slope
ACC 3466	24.2	-21.7	1.2	0.95	dense side, upper slope
ACC 3436	21.8	-24.4	1.08	1.07	crest
ACC 3492	+/-23.0*		1.0	1.0	box: 1st recording
ACC 3477	20.1	-22.8	1.00	1.00	ref: base of embankment,
ACC 5717	+/-17.0*		0.85	0.75	mid-height, core (drifting signal)
ACC 3492	+/-26.1*		1.3	1.15	box: 2nd recording

* corrected value, based on mean of peak positive and peak negative values

Table 5: Peak accelerations, GEM 2 earthquake 1

GEM 2 earthquake 2	Peak +ve (%)	Peak -ve (%)	Amplification (+ve)	Amplification (-ve)	Comments
ACC 1932	not reliable	not reliable			dense side, mid-slope
ACC 3466	29.3	-25.8	1.23	1.05	dense side, upper slope
ACC 3436	29.5	-26.8	1.23	1.09	crest
ACC 3492	24.0	-27.1	1.0	1.10	box: 1st recording
ACC 3477	23.9	-24.6	1.00	1.00	ref: base of embankment,
ACC 5717	+/-21.0*		0.88	0.85	mid-height, core (drifting signal)
ACC 3492	25.6	-27.9	1.07	1.13	box: 2nd recording

* corrected value, based on mean of peak positive and peak negative values

Table 6: Peak accelerations, GEM 2 earthquake 2

GEM 1 f_{nat} (Hz)	loose pocket	toe, loose side	core, mid-height	core, base of embankment	dense side, base
	ACC 5754	ACC 3441	ACC 1932	ACC 1552	ACC 3436
earthquake 1	8.8	15.5	12.4	21.0	17.5
earthquake 2	7.0	13.0	8.8	19.1	15.7
earthquake 3	6.8	12.3	7.9	18.3	15.2

GEM 2 f_{nat} (Hz)	crest of embankment	core, mid-height	core, base of embankment	dense side, top of slope	dense side, mid-slope
	ACC 3436	ACC 5717	ACC 3477	ACC 3466	ACC 1932
earthquake 1	3.7	9.7	5.7	7.3	5.0
earthquake 2	3.4	9.3			4.9

Table 7: Natural frequency of the embankment in GEM 1 and GEM 2 (prototype values)

GEM	Run	Horizontal/ vertical acceleration (%g)	Excess pore pressure	Factor of safety	Side of embankment
GEM 1	121	12 / 0	none	1.00	either
GEM 2	221	23 / 0	increased by 30 KPa in loose pocket	0.75	dense
GEM 2	222	23 / 0	increased by 30 KPa in loose pocket	0.56	loose
GEM 3	311	18 / 0	high increased piezometric values caused computation problems	no solution	na
GEM 3	312	18 / 0	Ru = 1.0 in loose zone, based on eq 2; deep seated slip	1.56	neither
GEM 3	411	23 / 5	none	0.84	loose
GEM 4	412	23 / 5	none	0.84	dense
GEM 4	413	23 / 5	Ru = 0.52 in middle dense zone, 0.87 in lower dense zone, 0.78 in loose zone, based on eq 3	1.26	loose
GEM 5	511	25 / 5	none	0.72	loose
GEM 5	512	25 / 5	none	0.83	dense
GEM 5	513	25 / 5	Ru = 0.8 in middle dense zone, 0.85 in lower dense zone, 0.95 in loose zone, based on eq 3	0.82	loose
GEM 6	611	21 / 5	none	0.83	loose
GEM 6	612	21 / 5	none	0.94	dense

Table 8: Summary of *Slope* analyses

GEM 3 earthquake 1	Peak +ve (%)	Peak -ve (%)	Amplification (+ve)	Amplification (-ve)	Comments
ACC 3477	13.3	-13.0	0.71	0.84	crest (isolated)
ACC 3492	9.7	-13.2	0.52	0.86	loose side, mid slope (slip)
ACC 1225	8.5	-15.7	0.45	1.02	mid-height, core (drifting signal)
ACC 1926	12.2	-15.9	0.65	1.03	loose zone (slip)
ACC 5754					na (base of embankment)
ACC 3436	18.8	-15.4	1.00	1.00	box: 1st recording
ACC 5701	28.4	-18.7	1.51	1.21	dense side, mid slope (slip)
ACC 3436	19.7	-16.9	1.05	1.10	box: 2nd recording

Table 9: Peak accelerations, GEM 3 earthquake 1

GEM 3 earthquake 2	Peak +ve (%)	Peak -ve (%)	Amplification (+ve)	Amplification (-ve)	Comments
ACC 3477	13.8	-17.2	0.80	0.97	crest (slip)
ACC 3492	11.9	-20.1	0.69	1.13	loose side, mid slope (slip)
ACC 1225	7.4	-19.1	0.43	1.07	mid-height, core (drifting signal)
ACC 1926	16.9	-21.1	0.98	1.19	loose zone (slip)
ACC 5754					na (base of embankment)
ACC 3436	17.2	-17.8	1.00	1.00	box: 1st recording
ACC 5701	78.5	-24.6	4.56	1.38	dense side, mid slope (slip)
ACC 3436	18.4	-18.1	1.07	1.02	box: 2nd recording

Table 10: Peak accelerations, GEM 3 earthquake 2

GEM 3 earthquake 3

	Peak +ve (%)	Peak -ve (%)	Amplification (+ve)	Amplification (-ve)	Comments
ACC 3477	16.0	-26.9	0.80	1.29	crest (slip)
ACC 3492	11.0	-23.6	0.55	1.13	loose side, mid slope (slip)
ACC 1225	10.3	-22.9	0.52	1.10	mid-height, core (drifting signal)
ACC 1926	14.6	-35.0	0.73	1.68	loose zone (slip)
ACC 5754					na (base of embankment)
ACC 3436	19.9	-20.8	1.00	1.00	box: 1st recording
ACC 5701	90.7	-26.8	4.56	1.29	dense side, mid slope (slip)
ACC 3436	19.4	-22.0	0.97	1.06	box: 2nd recording

Table 11: Peak accelerations, GEM 3 earthquake 3

GEM 3 earthquake 4

	Peak +ve (%)	Peak -ve (%)	Amplification (+ve)	Amplification (-ve)	Comments
ACC 3477	17.2	-40.9	0.84	1.86	crest (slip)
ACC 3492	10.9	-26.1	0.53	1.19	loose side, mid slope (slip)
ACC 1225	13.2	-31.2	0.65	1.42	mid-height, core (drifting signal)
ACC 1926	15.7	-39.8	0.77	1.81	loose zone (slip)
ACC 5754					na (base of embankment)
ACC 3436	20.4	-22.0	1.00	1.00	box: 1st recording
ACC 5701	99.0	-27.3	4.85	1.24	dense side, mid slope (slip)
ACC 3436	21.5	-21.3	1.05	0.97	box: 2nd recording

Table 12: Peak accelerations, GEM 3 earthquake 4

GEM 4 earthquake 1

	Peak +ve (%)	Peak -ve (%)	Amplification (+ve)	Amplification (-ve)	Comments
ACC 5701	21.5	-13.0	0.85	0.83	crest
ACC 1926	19.2	-14.4	0.76	0.92	loose side, mid slope
ACC 3492	14.9	-16.2	0.59	1.04	loose zone
ACC 3477	25.3	-15.6	1.00	1.00	base of embankment
ACC 1900	5.1	-5.7	0.20	0.37	box (vertical)
ACC 3436	15.0	-15.2	0.59	0.97	box: 1st recording
ACC 3441	16.8	-15.7	0.66	1.01	mid-height, core
ACC 1932	not reliable				dense side mid slope
ACC 3436	20.7	-16.7	0.82	1.07	box: 2nd recording

Table 13: Peak accelerations, GEM 4 earthquake 1

GEM 4 earthquake 2

	Peak +ve (%)	Peak -ve (%)	Amplification (+ve)	Amplification (-ve)	Comments
ACC 5701	27.5	-14.2	0.83	0.59	crest
ACC 1926					na
ACC 3492	39.2	-17.7	1.18	0.73	loose zone
ACC 3477	33.1	-24.1	1.00	1.00	base of embankment
ACC 1900	6.3	-6.6	0.19	0.28	box (vertical)
ACC 3436	21.2	-20.1	0.64	0.83	box: 1st recording
ACC 3441	35.1	-19.5	1.06	0.81	mid-height, core
ACC 1932	not reliable				dense side mid slope
ACC 3436	28.9	-23.6	0.87	0.98	box: 2nd recording

Table 14: Peak accelerations, GEM 4 earthquake 2

GEM 4 earthquake 3					
	Peak +ve (%)	Peak -ve (%)	Amplification (+ve)	Amplification (-ve)	Comments
ACC 5701	30.7	-15.8	0.92	0.61	crest
ACC 1926					na
ACC 3492	29.5	-17.9	0.88	0.69	loose zone
ACC 3477	33.5	-26.1	1.00	1.00	base of embankment
ACC 1900	5.2	-6.9	0.16	0.26	box (vertical)
ACC 3436	24.3	-22.2	0.73	0.85	box: 1st recording
ACC 3441	47.1	-16.5	1.41	0.63	mid-height, core
ACC 1932	not reliable				dense side mid slope
ACC 3436	25.7	-23.2	0.77	0.89	box: 2nd recording

Table 15: Peak accelerations, GEM 4 earthquake 3

GEM 4 earthquake 4					
	Peak +ve (%)	Peak -ve (%)	Amplification (+ve)	Amplification (-ve)	Comments
ACC 5701	34.0	-18.7	0.89	0.54	crest
ACC 1926					na
ACC 3492	38.4	-16.9	1.00	0.49	loose zone
ACC 3477	38.4	-34.7	1.00	1.00	base of embankment
ACC 1900	6.7	-9.2	0.17	0.27	box (vertical)
ACC 3436	27.2	-27.6	0.71	0.80	box: 1st recording
ACC 3441	65.1	-20.4	1.70	0.59	mid-height, core
ACC 1932	not reliable				dense side mid slope
ACC 3436	28.5	-25.1	0.74	0.72	box: 2nd recording

Table 16: Peak accelerations, GEM 4 earthquake 4

GEM 5 earthquake 1	Peak +ve (%)	Peak -ve (%)	Amplification (+ve)	Amplification (-ve)	Comments
ACC 3441	5.6	-6.2	0.25	0.42	crest
ACC 3492	15.5	-13.6	0.70	0.93	loose zone mid slope
ACC 3477	15.4	-14.9	0.70	1.01	loose zone base
ACC 5701	22.1	-14.7	1.00	1.00	base of embankment
ACC 1900	5.9	-6.2	0.27	0.42	box (vertical)
ACC 3436	17.5	-16.7	0.79	1.14	box: 1st recording
ACC 1572	9.4	-29.6	0.43	2.01	dense side mid slope
ACC 1932	na	na			mid-height, core
ACC 3436	18.6	-18.3	0.84	1.24	box: 2nd recording

Table 17: Peak accelerations, GEM 5 earthquake 1

GEM 5 earthquake 2	Peak +ve (%)	Peak -ve (%)	Amplification (+ve)	Amplification (-ve)	Comments
ACC 3441	9.5	-5.8	0.27	0.26	crest
ACC 3492	29.6	-16.2	0.85	0.72	loose zone mid slope
ACC 3477	21.3	-22.1	0.61	0.98	loose zone base
ACC 5701	35.0	-22.5	1.00	1.00	base of embankment
ACC 1900	6.0	-7.1	0.17	0.31	box (vertical)
ACC 3436	22.9	-23.4	0.65	1.04	box: 1st recording
ACC 1572	18.8	-37.8	0.54	1.68	dense side mid slope
ACC 1932	na	na			mid-height, core
ACC 3436	24.1	-23.0	0.69	1.02	box: 2nd recording

Table 18: Peak accelerations, GEM 5 earthquake 2

GEM 5 earthquake 3

	Peak +ve (%)	Peak -ve (%)	Amplification (+ve)	Amplification (-ve)	Comments
ACC 3441	9.7	-6.2	0.29	0.21	crest
ACC 3492	42.4	-17.7	1.27	0.60	loose zone mid slope
ACC 3477	21.3	-22.3	0.64	0.76	loose zone base
ACC 5701	33.3	-29.3	1.00	1.00	base of embankment
ACC 1900	6.3	-8.4	0.19	0.29	box (vertical)
ACC 3436	25.2	-26.4	0.76	0.90	box: 1st recording
ACC 1572	13.8	-74.2*	0.41	2.53	dense side mid slope
ACC 1932	na	na			mid-height, core
ACC 3436	25.9	-28.3	0.78	0.97	box: 2nd recording

* interpretation of this value is unclear

Table 19: Peak accelerations, GEM 5 earthquake 3

GEM 5 earthquake 4

	Peak +ve (%)	Peak -ve (%)	Amplification (+ve)	Amplification (-ve)	Comments
ACC 3441	8.9	-6.4	0.24	0.19	crest
ACC 3492	49.7	-16.8	1.35	0.51	loose zone mid slope
ACC 3477	26.3	-25.4	0.71	0.77	loose zone base
ACC 5701	36.9	-33.2	1.00	1.00	base of embankment
ACC 1900	7.8	-7.4	0.21	0.22	box (vertical)
ACC 3436	26.2	-28.5	0.71	0.86	box: 1st recording
ACC 1572	4.4	-83.6*	0.12	2.52	dense side mid slope
ACC 1932	na	na			mid-height, core
ACC 3436	27.6	-29.9	0.75	0.90	box: 2nd recording

* interpretation of this value is unclear

Table 20: Peak accelerations, GEM 5 earthquake 4

GEM 6 earthquake 1	Peak +ve (%)	Peak -ve (%)	Amplification (+ve)	Amplification (-ve)	Comments
ACC 3466	28.7	-10.2	2.02	0.71	crest
ACC 1900	8.0	-16.5	0.57	1.15	loose side mid slope
ACC 3477	16.3	-11.2	1.15	0.78	mid-height, core
ACC 3492	13.4	-10.6	0.94	0.74	loose zone
ACC 5701	14.2	-14.4	1.00	1.00	base of embankment box (vertical)
ACC 3436	11.3	-12.7	0.80	0.88	box: 1st recording
ACC 1572	12.5	-8.6	0.88	0.66	crest (vertical)
ACC 3441	25.9*	-39.7*	1.82	2.76	dense side mid slope
ACC 3436	11.1	-13.1	0.78	0.91	box: 2nd recording

* numerical values seem disproportionately high

Table 21: Peak accelerations, GEM 6 earthquake 1

GEM 6 earthquake 2	Peak +ve (%)	Peak -ve (%)	Amplification (+ve)	Amplification (-ve)	Comments
ACC 3466	32.2	-12.2	1.48	0.60	crest
ACC 1900	10.3	-22.6	0.47	1.12	loose side mid slope
ACC 3477	27.5	-10.8	1.26	0.53	mid-height, core
ACC 3492	25.7	-14.6	1.18	0.72	loose zone
ACC 5701	21.8	-20.2	1.00	1.00	base of embankment box (vertical)
ACC 3436	18.4	-17.9	0.84	0.89	box: 1st recording
ACC 1572	14.2	-8.9	0.65	0.44	crest (vertical)
ACC 3441	38.3*	-71.1*	1.76	3.52	dense side mid slope
ACC 3436	18.6	-18.7	0.85	0.93	box: 2nd recording

* numerical values seem disproportionately high

Table 22: Peak accelerations, GEM 6 earthquake 2

GEM 6 earthquake 3

	Peak +ve (%)	Peak -ve (%)	Amplification (+ve)	Amplification (-ve)	Comments
ACC 3466	39.0	-11.8	1.56	0.50	crest
ACC 1900	12.2	-27.6	0.49	1.16	loose side mid slope
ACC 3477	34.8	-11.4	1.39	0.48	mid-height, core
ACC 3492	30.1	-18.3	1.20	0.77	loose zone
ACC 5701	25.0	-23.7	1.00	1.00	base of embankment box (vertical)
ACC 3436	21.0	-20.4	0.84	0.86	box: 1st recording
ACC 1572	16.4	-16.6	0.66	0.70	crest (vertical)
ACC 3441	41.3*	-108.0*	1.65	4.56	dense side mid slope
ACC 3436	22.2	-21.3	0.89	0.90	box: 2nd recording

* numerical values seem disproportionately high

Table 23: Peak accelerations, GEM 6 earthquake 3

GEM 6 earthquake 4

	Peak +ve (%)	Peak -ve (%)	Amplification (+ve)	Amplification (-ve)	Comments
ACC 3466	42.5	-13.3	1.48	0.48	crest
ACC 1900	12.0	-36.4	0.42	1.32	loose side mid slope
ACC 3477	43.4	-14.0	1.51	0.51	mid-height, core
ACC 3492	33.7	-23.2	1.17	0.84	loose zone
ACC 5701	28.8	-27.6	1.00	1.00	base of embankment box (vertical)
ACC 3436	23.1	-22.1	0.80	0.80	box: 1st recording
ACC 1572	19.6	-17.0	0.68	0.62	crest (vertical)
ACC 3441	48.4*	-150.0*	1.68	5.43	dense side mid slope
ACC 3436	25.1	-24.9	0.87	0.90	box: 2nd recording

* numerical values seem disproportionately high

Table 24: Peak accelerations, GEM 6 earthquake 4

GEM 121
tbc

SIR ALEXANDER GIBB AND PARTNERS LTD.

Program: SLOPE Version 8.23 Revision A13.B12.R22
Licensed from GEOSOLVE

usa EMBANKMENT FAILURES
earthquake induced liquefaction (centrifuge study)

Sheet No.
Run No.
Job No.
Made by :
Date: 15-
Checked :

Units: kN,m

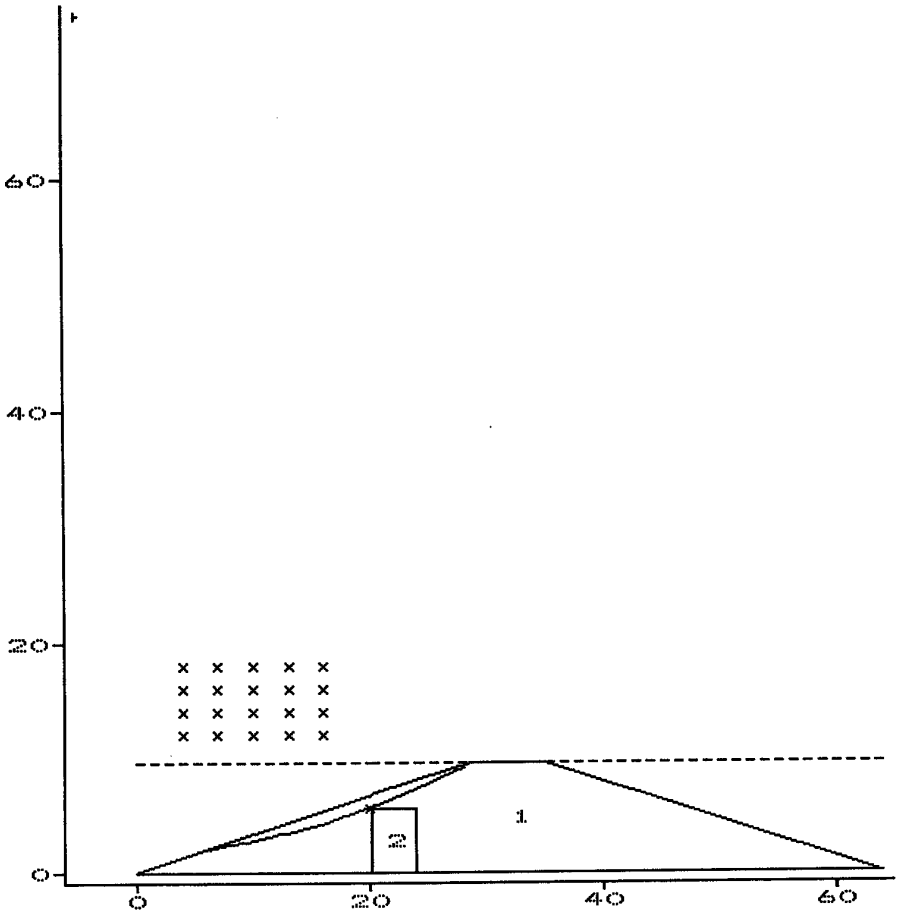

Scale = 1 : 604

--- S t r a t u m --- No.	Description	Bulk unit wt. below GWL kN/m3	above GWL kN/m3	-------Strength parameters--- C kN/m2	Phi (deg)	dC/dY kN/m2/m	D f
1	medium dense sand	19.10	19.10	0.00	32.00		
2	loose sand	19.10	19.10	0.00	30.00		
3	medium dense sand	19.10	19.10	0.00	32.00		

Factor of safety = 0.995

Centre of circle: X = -5.00 Y = 74.00 Radius = 72.83

Figure 1: *Slope* analysis of GEM 1

GEM 22

SIR ALEXANDER GIBB AND PARTNERS LTD.

Program: SLOPE Version 8.23 Revision A13.B12.R22
Licensed from GEOSOLVE

usa EMBANKMENT FAILURES
earthquake induced liquefaction (centrifuge study)

Sheet No.
Run No.
Job No.
Made by :
Date: 15-
Checked :

Units: kN,m

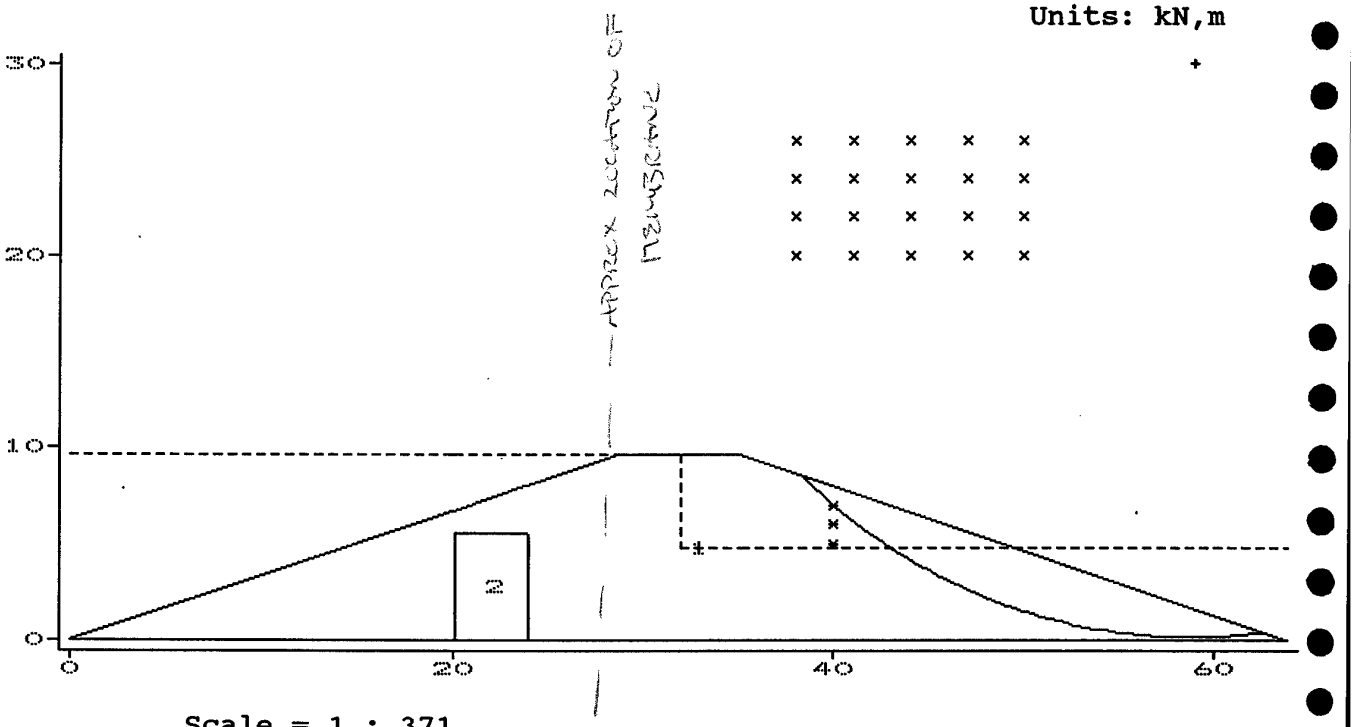

Scale = 1 : 371

--- S t r a t u m ---		Bulk unit wt. below GWL	above GWL	-------Strength parameters--- C	Phi	dC/dY	D f
No.	Description	kN/m3	kN/m3	kN/m2	(deg)	kN/m2/m	
1	medium dense sand	18.90	18.90	0.00	31.00		
2	loose sand	19.00	19.00	0.00	30.00	Piezometric sur	
3	medium dense sand	18.90	18.90	0.00	31.00		

Factor of safety = 0.752

Centre of circle: X = 59.00 Y = 30.00 Radius = 29.83

PP IN LOOSE ZONE INCREASED BY 30kPa
(PEAK RISE DURING SHK)

Figure 2: *Slope* analysis of GEM 2

GEM 2 2

SIR ALEXANDER GIBB AND PARTNERS LTD.

Program: SLOPE Version 8.23 Revision A13.B12.R22
Licensed from GEOSOLVE

usa EMBANKMENT FAILURES
earthquake induced liquefaction (centrifuge study)

Sheet No.
Run No.

Job No.
Made by :
Date: 15-
Checked :

Units: kN,m

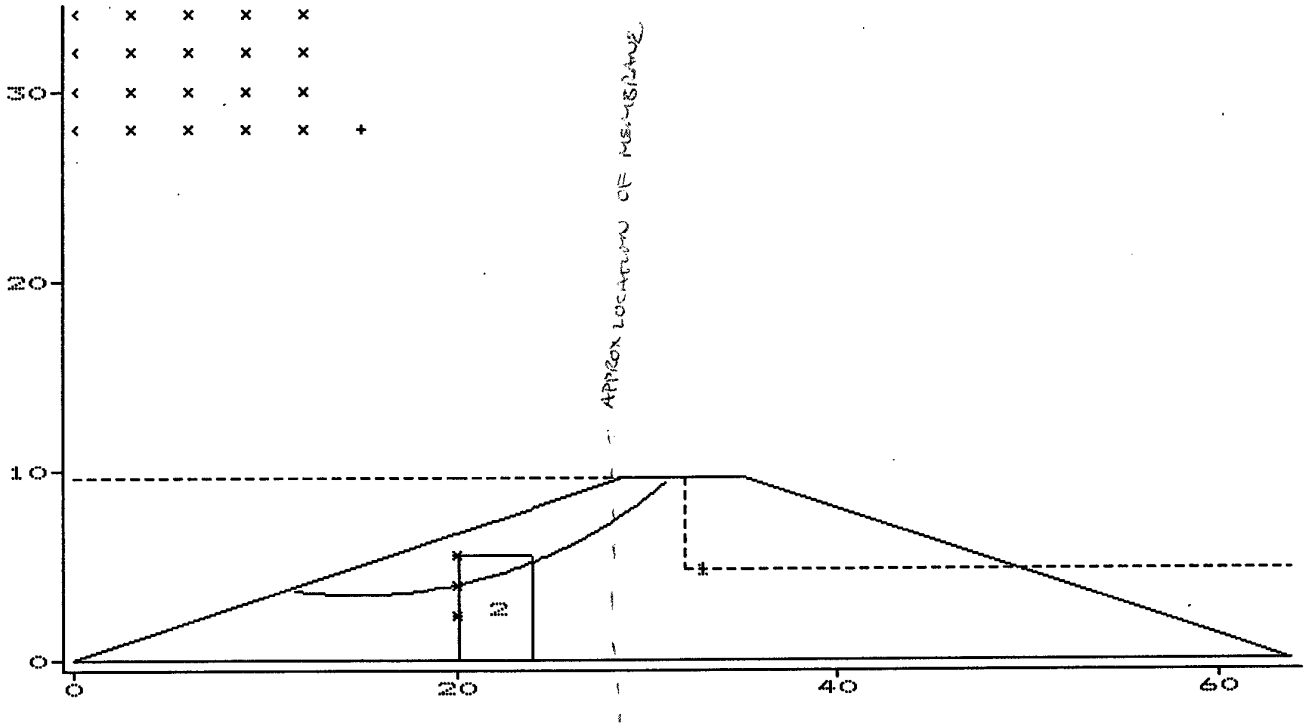

Scale = 1 : 371

--- S t r a t u m --- No.	Description	Bulk unit wt. below GWL kN/m3	above GWL kN/m3	C kN/m2	Phi (deg)	dC/dY kN/m2/m	D f
1	medium dense sand	18.90	18.90	0.00	31.00		
2	loose sand	19.00	19.00	0.00	30.00	Piezometric sur	
3	medium dense sand	18.90	18.90	0.00	31.00		

Factor of safety = 0.558

Centre of circle: X = 15.00 Y = 28.00 Radius = 24.52

PP IN LOOSE ZONE INCREASED BY 30 kPa
(PEAK RISE DURING EQ)

Figure 3: *Slope* analysis of GEM 2

GEM 311

SIR ALEXANDER GIBB AND PARTNERS LTD.

Program: SLOPE Version 8.23 Revision A13.B12.R22
Licensed from GEOSOLVE

usa EMBANKMENT FAILURES
earthquake induced liquefaction (centrifuge study)

Sheet No.
Run No.
Job No.
Made by :
Date: 15-
Checked :

Units: kN,m

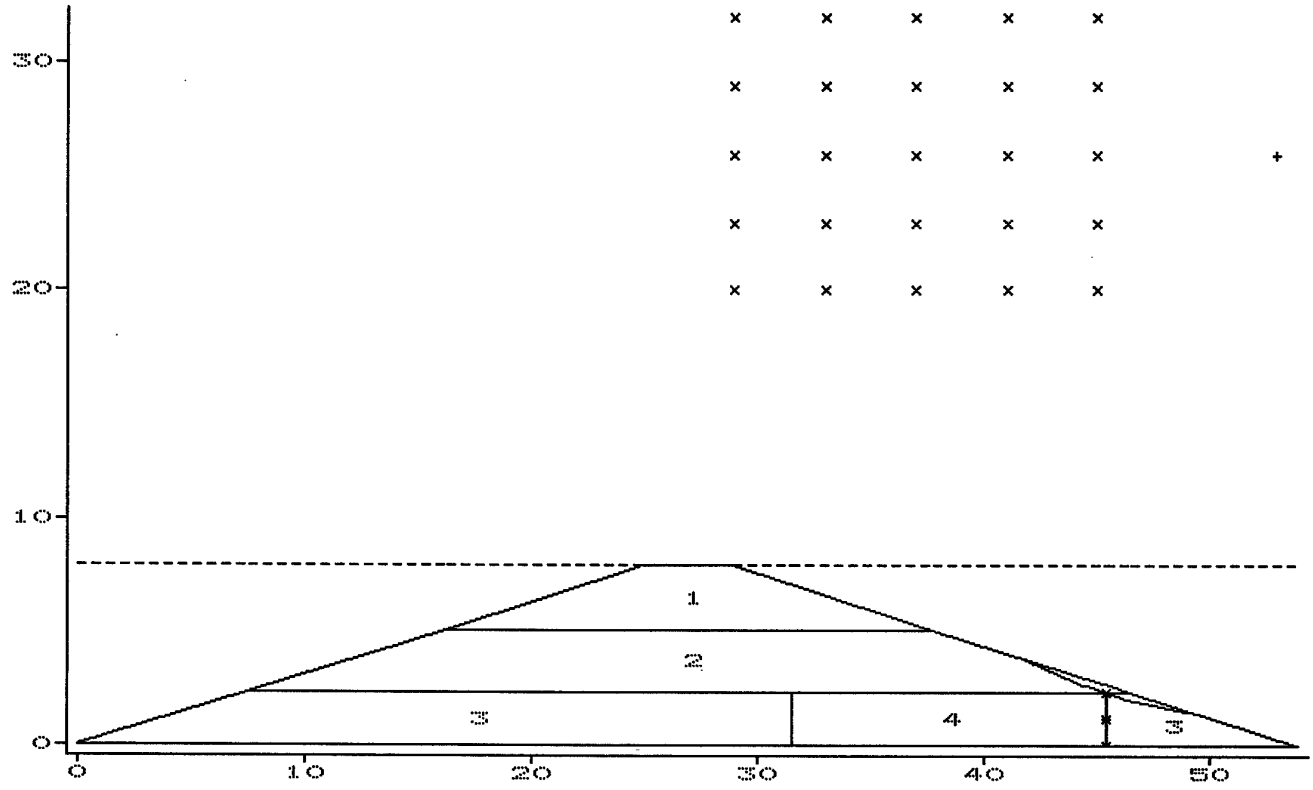

Scale = 1 : 313

--- S t r a t u m --- No.	Description	Bulk unit wt. below GWL kN/m3	above GWL kN/m3	-------Strength parameters--- C kN/m2	Phi (deg)	dC/dY kN/m2/m	D f
1	medium dense sand	19.10	19.10	0.00	32.00	Piezometric sur	
2	medium dense sand	19.10	19.10	0.00	32.00	Piezometric sur	
3	medium dense sand	19.10	19.10	0.00	32.00	Piezometric sur	
4	loose sand	18.90	18.90	0.00	29.00	Piezometric sur	
5	medium dense sand	19.10	19.10	0.00	32.00		

Figure 4: *Slope* analysis of GEM 3

SIR ALEXANDER GIBB AND PARTNERS LTD.

Program: SLOPE Version 8.23 Revision A13.B12.R22
Licensed from GEOSOLVE

usa EMBANKMENT FAILURES
earthquake induced liquefaction (centrifuge study)

Sheet No.
Run No. GEM312

Job No. J93039
Made by : GJBr
Date: 15-Feb-96
Checked :

Units: kN,m

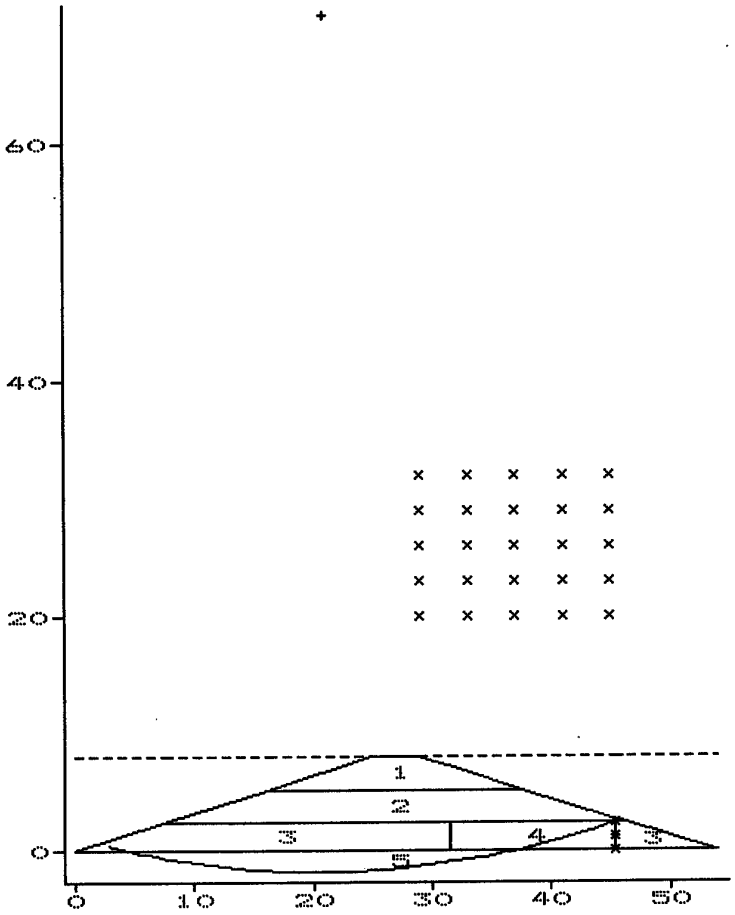

Scale = 1 : 594

--- S t r a t u m --- No.	Description	Bulk unit wt. below GWL kN/m3	above GWL kN/m3	C kN/m2	Phi (deg)	dC/dY kN/m2/m	Datum for C
1	medium dense sand	19.10	19.10	0.00	32.00		
2	medium dense sand	19.10	19.10	0.00	32.00		
3	medium dense sand	19.10	19.10	0.00	32.00		
4	loose sand	18.90	18.90	0.00	29.00	Ru = 1.000	
5	medium dense sand	19.10	19.10	0.00	32.00		

Factor of safety = 1.577

Centre of circle: X = 21.00 Y = 71.00 Radius = 72.81

Figure 5: *Slope* analysis of GEM 3

SIR ALEXANDER GIBB AND PARTNERS LTD.

Program: SLOPE Version 8.23 Revision A13.B12.R22
Licensed from GEOSOLVE

usa EMBANKMENT FAILURES
earthquake induced liquefaction (centrifuge study)

Sheet No.
Run No. GEM411

Job No. J93039
Made by : GJBr
Date: 15-Feb-96
Checked :

Units: kN,m

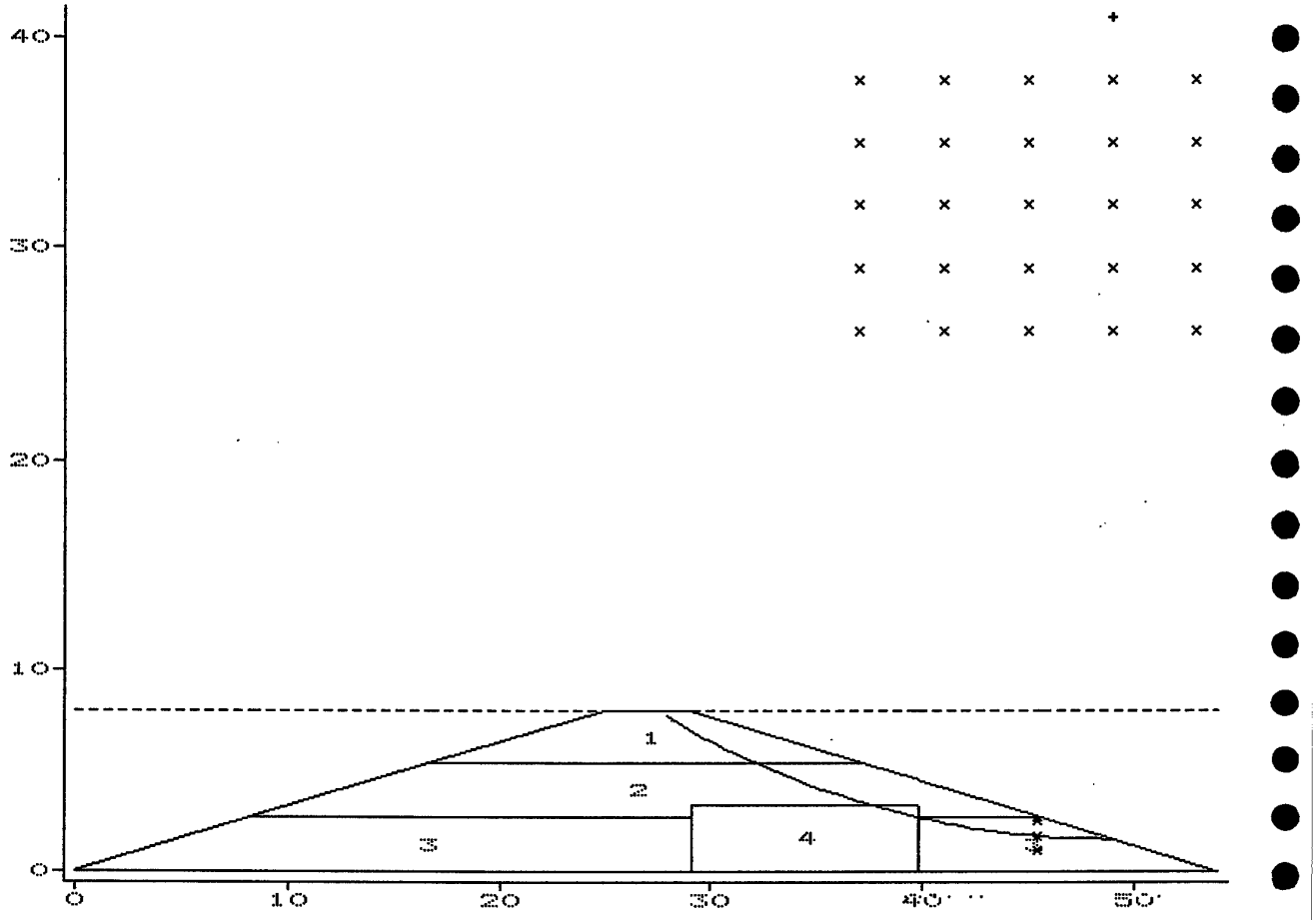

Scale = 1 : 334

--- S t r a t u m --- No.	Description	Bulk unit wt. below GWL kN/m3	above GWL kN/m3	-------Strength parameters------- C kN/m2	Phi (deg)	dC/dY kN/m2/m	Datum for C
1	medium dense sand	19.10	19.10	0.00	32.00	Piezometric surface 1	
2	medium dense sand	19.10	19.10	0.00	32.00	Piezometric surface 2	
3	medium dense sand	19.10	19.10	0.00	32.00	Piezometric surface 3	
4	loose sand	19.00	19.00	0.00	30.00	Piezometric surface 4	
5	medium dense sand	19.10	19.10	0.00	32.00		

Factor of safety = 0.841

Centre of circle: X = 49.00 Y = 41.00 Radius = 39.41

Figure 6: *Slope* analysis of GEM 3

SIR ALEXANDER GIBB AND PARTNERS LTD.

Program: SLOPE Version 8.23 Revision A13.B12.R22
Licensed from GEOSOLVE

usa EMBANKMENT FAILURES
earthquake induced liquefaction (centrifuge study)

Sheet No.
Run No. GEM412

Job No. J93039
Made by : GJBr
Date: 15-Feb-96
Checked :

Units: kN,m

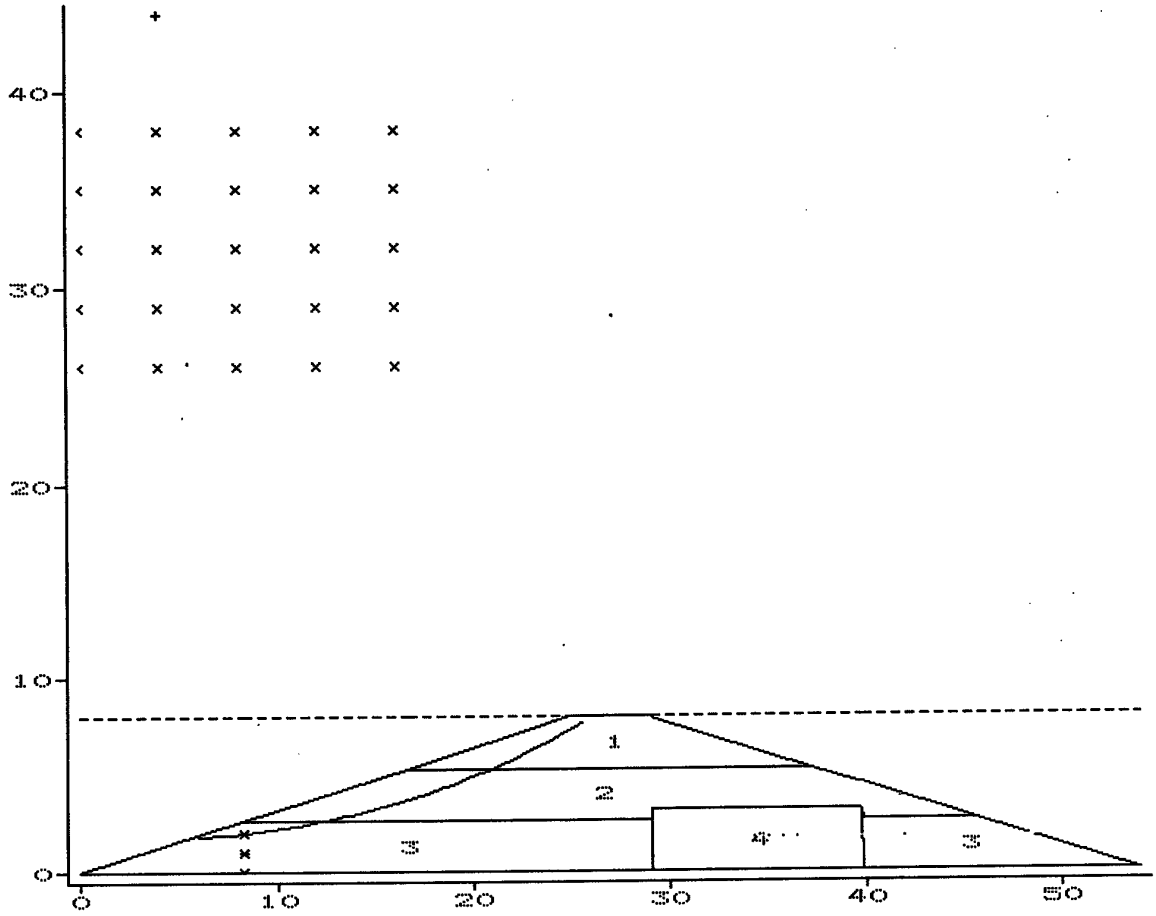

Scale = 1 : 359

--- S t r a t u m --- No.	Description	Bulk unit wt. below GWL kN/m3	above GWL kN/m3	-------Strength parameters----- C kN/m2	Phi (deg)	dC/dY kN/m2/m	Dat for
1	medium dense sand	19.10	19.10	0.00	32.00	Piezometric surfa	
2	medium dense sand	19.10	19.10	0.00	32.00	Piezometric surfa	
3	medium dense sand	19.10	19.10	0.00	32.00	Piezometric surfa	
4	loose sand	19.00	19.00	0.00	30.00	Piezometric surfa	
5	medium dense sand	19.10	19.10	0.00	32.00		

Factor of safety = 0.844

Centre of circle: X = 4.00 Y = 44.00 Radius = 42.22

Figure 7: *Slope* analysis of GEM 4

GEM 413

SIR ALEXANDER GIBB AND PARTNERS LTD.

Program: SLOPE Version 8.23 Revision A13.B12.R22
Licensed from GEOSOLVE

usa EMBANKMENT FAILURES
earthquake induced liquefaction (centrifuge study)

Sheet No.
Run No.
Job No.
Made by :
Date: 15-
Checked :

Units: kN,m

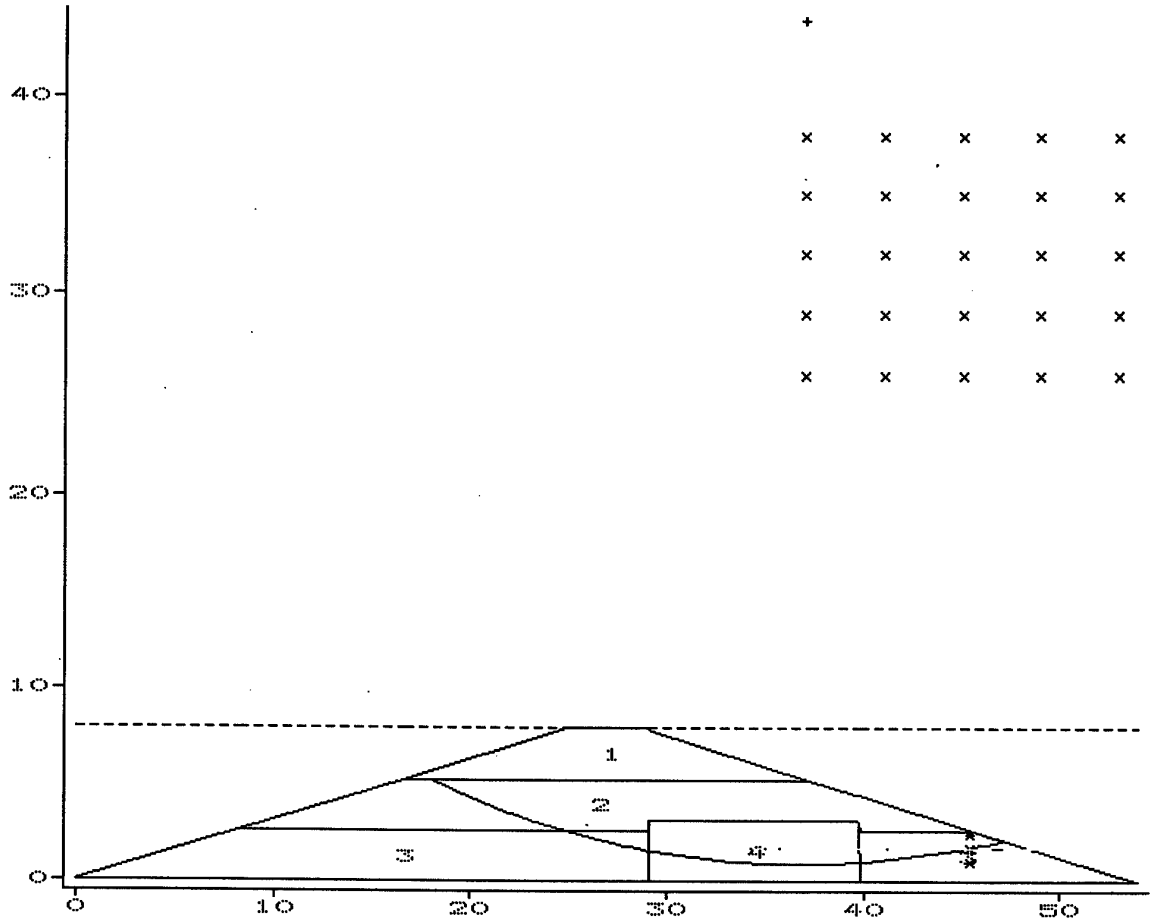

Scale = 1 : 359

--- S t r a t u m --- No.	Description	Bulk unit wt. below GWL kN/m3	above GWL kN/m3	-------Strength parameters--- C kN/m2	Phi (deg)	dC/dY kN/m2/m	D f
1	medium dense sand	19.10	19.10	0.00	32.00		
2	medium dense sand	19.10	19.10	0.00	32.00	Ru = 0.520	
3	medium dense sand	19.10	19.10	0.00	32.00	Ru = 0.820	
4	loose sand	19.00	19.00	0.00	30.00	Ru = 0.780	
5	medium dense sand	19.10	19.10	0.00	32.00		

Factor of safety = 1.256

Centre of circle: X = 37.00 Y = 44.00 Radius = 43.08

Figure 8: *Slope* analysis of GEM 4

GEM 511

SIR ALEXANDER GIBB AND PARTNERS LTD.

Program: SLOPE Version 8.23 Revision A13.B12.R22
Licensed from GEOSOLVE

usa EMBANKMENT FAILURES
earthquake induced liquefaction (centrifuge study)

Sheet No.
Run No.
Job No.
Made by :
Date: 15-
Checked :

Units: kN,m

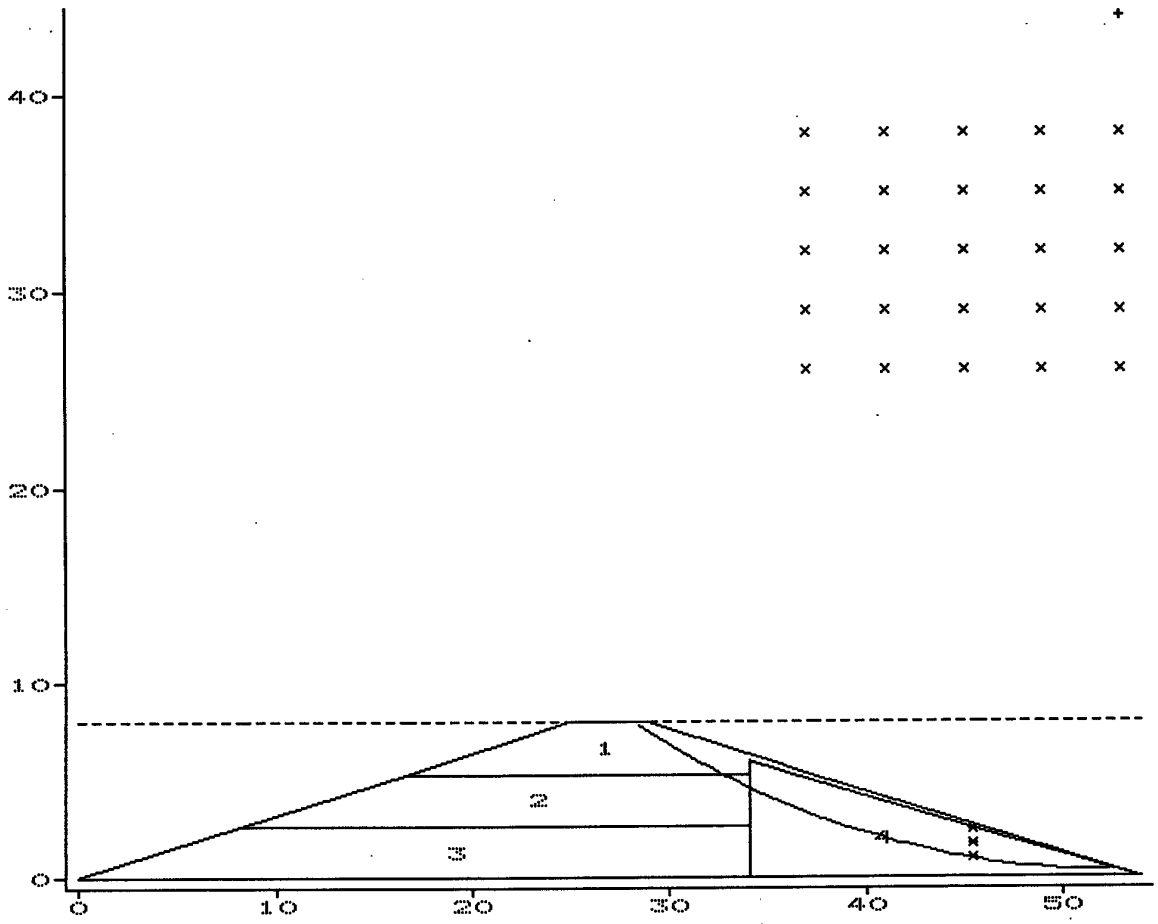

Scale = 1 : 359

--- S t r a t u m --- No.	Description	Bulk unit wt. below GWL kN/m3	above GWL kN/m3	-------Strength parameters--- C kN/m2	Phi (deg)	dC/dY kN/m2/m	D f
1	medium dense sand	19.30	19.30	0.00	33.00	Piezometric sur	
2	medium dense sand	19.30	19.30	0.00	33.00	Piezometric sur	
3	medium dense sand	19.30	19.30	0.00	33.00	Piezometric sur	
4	loose sand	18.80	18.80	0.00	29.00	Piezometric sur	
5	medium dense sand	19.30	19.30	0.00	33.00		

Factor of safety = 0.721

Centre of circle: X = 53.00 Y = 44.00 Radius = 43.67

Figure 9: *Slope* analysis of GEM 5

GEM 512

SIR ALEXANDER GIBB AND PARTNERS LTD.

Program: SLOPE Version 8.23 Revision A13.B12.R22
Licensed from GEOSOLVE

usa EMBANKMENT FAILURES
earthquake induced liquefaction (centrifuge study)

Sheet No.
Run No.
Job No.
Made by :
Date: 15-
Checked :

Units: kN,m

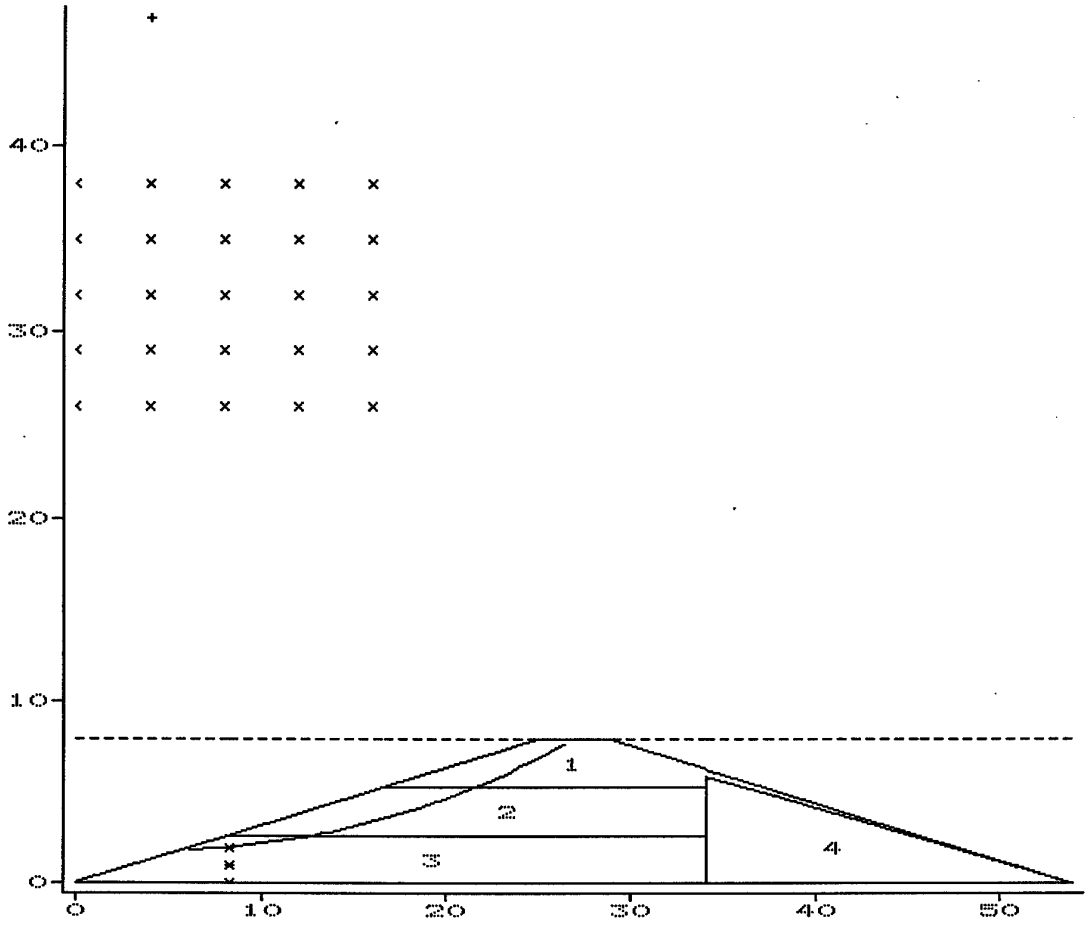

Scale = 1 : 383

--- S t r a t u m --- No.	Description	Bulk unit wt. below GWL kN/m3	above GWL kN/m3	-------Strength parameters--- C kN/m2	Phi (deg)	dC/dY kN/m2/m	D f
1	medium dense sand	19.30	19.30	0.00	33.00	Piezometric sur	
2	medium dense sand	19.30	19.30	0.00	33.00	Piezometric sur	
3	medium dense sand	19.30	19.30	0.00	33.00	Piezometric sur	
4	loose sand	18.80	18.80	0.00	29.00	Piezometric sur	
5	medium dense sand	19.30	19.30	0.00	33.00		

Factor of safety = 0.832

Centre of circle: X = 4.00 Y = 47.00 Radius = 45.20

Figure 10: *Slope* analysis of GEM 5

SIR ALEXANDER GIBB AND PARTNERS LTD.

Program: SLOPE Version 8.23 Revision A13.B12.R22
Licensed from GEOSOLVE

usa EMBANKMENT FAILURES
earthquake induced liquefaction (centrifuge study)

Sheet No.
Run No. GEM513

Job No. J93039
Made by : GJBr
Date: 15-Feb-96
Checked :

Units: kN,m

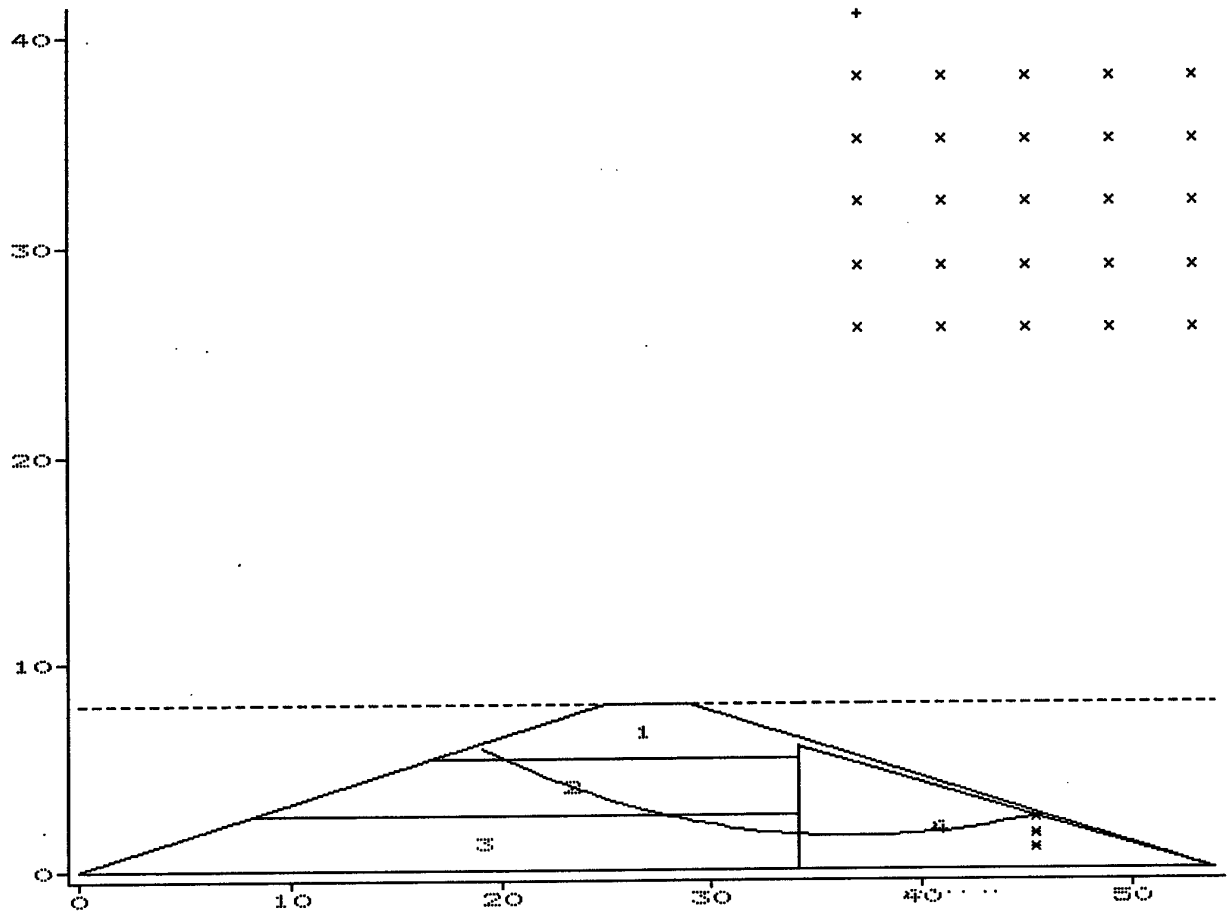

Scale = 1 : 334

--- S t r a t u m ---		Bulk unit wt. below GWL	above GWL	C	Phi	dC/dY	Datum for C
No.	Description	kN/m3	kN/m3	kN/m2	(deg)	kN/m2/m	
1	medium dense sand	19.30	19.30	0.00	33.00		
2	medium dense sand	19.30	19.30	0.00	33.00	Ru = 0.800	
3	medium dense sand	19.30	19.30	0.00	33.00	Ru = 0.850	
4	loose sand	18.80	18.80	0.00	29.00	Ru = 0.950	
5	medium dense sand	19.30	19.30	0.00	33.00		

Factor of safety = 0.822

Centre of circle: X = 37.00 Y = 41.00 Radius = 39.41

Figure 11: *Slope* analysis of GEM 5

SIR ALEXANDER GIBB AND PARTNERS LTD.

Program: SLOPE Version 8.23 Revision A13.B12.R22
Licensed from GEOSOLVE

usa EMBANKMENT FAILURES
earthquake induced liquefaction (centrifuge study)

Sheet No.
Run No. GEM611

Job No. J93039
Made by : GJBr
Date: 15-Feb-96
Checked :

Units: kN,m

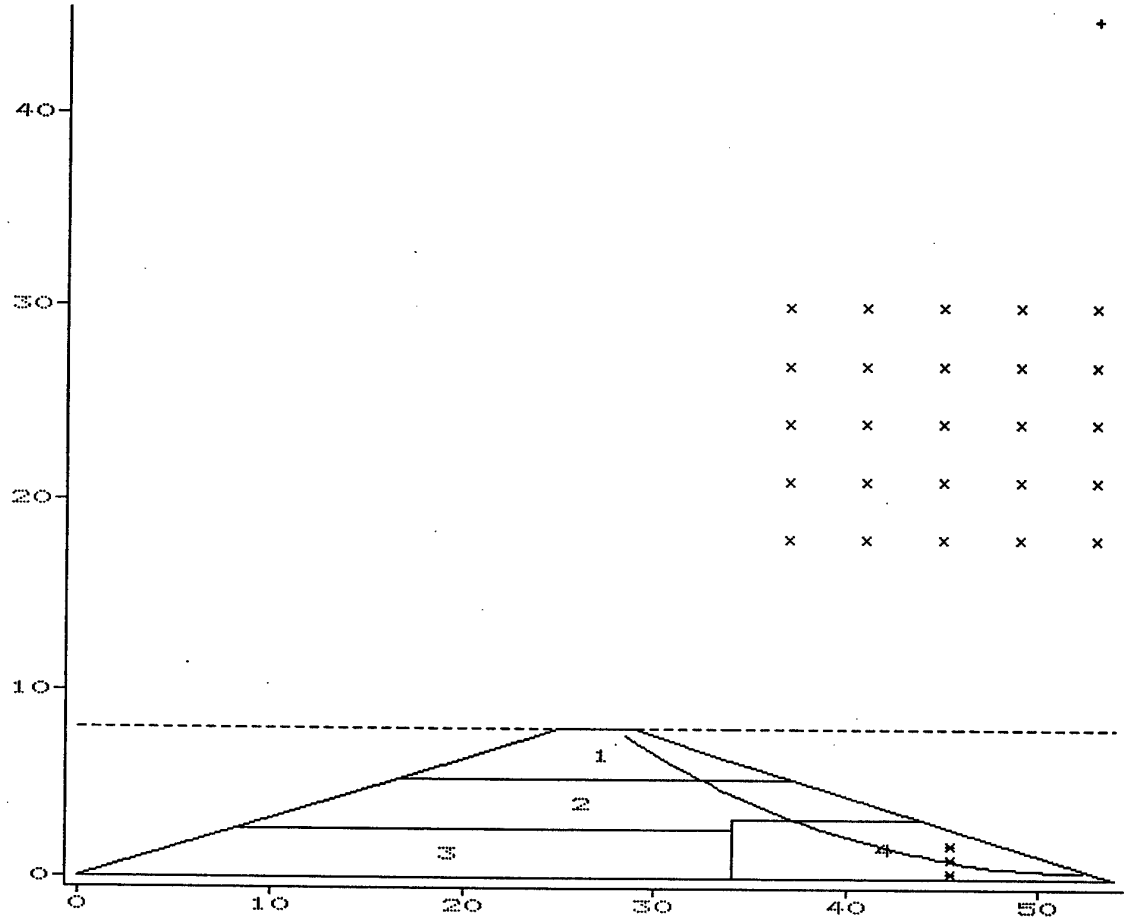

Scale = 1 : 367

--- S t r a t u m ---		Bulk unit wt. below GWL	above GWL	C	Phi	-------Strength parameters------- dC/dY	Datum for C
No.	Description	kN/m3	kN/m3	kN/m2	(deg)	kN/m2/m	
1	medium dense sand	19.30	19.30	0.00	33.00	Piezometric surface 1	
2	medium dense sand	19.30	19.30	0.00	33.00	Piezometric surface 2	
3	medium dense sand	19.30	19.30	0.00	33.00	Piezometric surface 3	
4	loose sand	18.80	18.80	0.00	29.00	Piezometric surface 4	
5	medium dense sand	19.30	19.30	0.00	33.00		

Factor of safety = 0.828

Centre of circle: X = 53.00 Y = 45.00 Radius = 44.65

Figure 12: *Slope* analysis of GEM 6

SIR ALEXANDER GIBB AND PARTNERS LTD.

Program: SLOPE Version 8.23 Revision A13.B12.R22
Licensed from GEOSOLVE

usa EMBANKMENT FAILURES
earthquake induced liquefaction (centrifuge study)

Sheet No.
Run No. GEM612

Job No. J93039
Made by : GJBr
Date: 15-Feb-96
Checked :

Units: kN,m

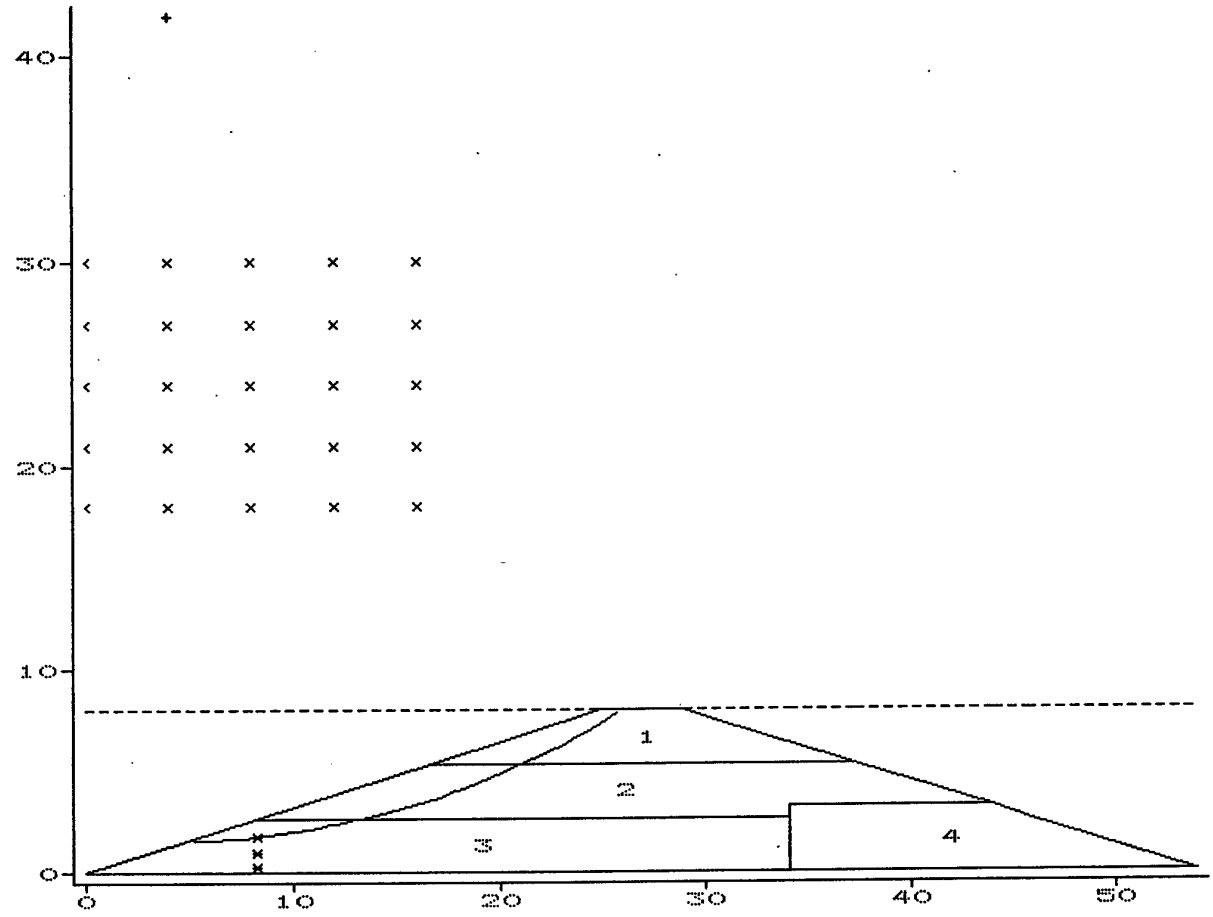

Scale = 1 : 343

--- S t r a t u m ---		Bulk unit wt. below GWL	above GWL	C	Phi	dC/dY	Datum for C
No.	Description	kN/m3	kN/m3	kN/m2	(deg)	kN/m2/m	
1	medium dense sand	19.30	19.30	0.00	33.00	Piezometric surface 1	
2	medium dense sand	19.30	19.30	0.00	33.00	Piezometric surface 2	
3	medium dense sand	19.30	19.30	0.00	33.00	Piezometric surface 3	
4	loose sand	18.80	18.80	0.00	29.00	Piezometric surface 4	
5	medium dense sand	19.30	19.30	0.00	33.00		

Factor of safety = 0.938

Centre of circle: X = 4.00 Y = 42.00 Radius = 40.48

Figure 13: *Slope* analysis of GEM 6

APPENDIX A

Slope stability calculations

The analysis method chosen was Janbu's method[A1] using parallel inclined interslice forces. In the case of circular slips this is identical to Spencer's method[A2]. Slope stability was examined under a combination of horizontal and vertical accelerations, and excess pore pressure (the accelerations being considered as applying quasi-static D'Alembert body forces). The piezometric changes were treated in two ways, firstly using actual values measured in the model and applying these to specific zones, and secondly by using the R_u capability in the *Slope* analysis to vary piezometric levels as a function of total stress (this approach causing fewer computational difficulties). In the first approach the magnitude of the excess pore pressures was taken from the long term traces presented in the data reports for the GEM series. These excess pore pressures were modelled by dividing the dense zone into three layers and raising the piezometric surface in each layer by the average excess pore pressure recorded by the pore pressure transducers that were located in these layers. The second approach modelled the rise in pore pressure by specifying an R_u value for each individual stratum, where $R_u = u / \sigma_v$ with u the pore pressure in the stratum and σ_v the total overburden stress.

For the submerged slopes in GEM 1 and GEM 2 the water was above ground level. The pressure of water acting on the ground surface was automatically taken into account by the program.

Circular slip surfaces were analysed by defining a rectangular grid of centres that was automatically extended to find the slip surface with the lowest factor of safety. Common points were selected to force the slip to pass through the toe of the slope, examining both upstream and downstream slopes. This prevented the program from selecting shallow surface failures.

The shear strength parameters were determined from the relative density after DJ D'Appolonia, E D'Appolonia and RF Brisette (1968)[A3]. The input excess pore pressures and accelerations have been chosen to be typical of a given set of earthquakes (eg GEM 1 earthquakes 1 to 3) rather than modelling one particular test. More emphasis was given to the values recorded in the latter tests of each set. Earthquake forces were modelled in a quasi static manner by defining horizontal and vertical acceleration coefficients E_h and E_v such that

[A1] Janbu N, Bjerrum L and Kjaernsli B (1956), Stability calculations for fillings, cuts and natural slopes, Norwegian Geotechnical Institute, Publication No 16.
[A2] Spencer E (1967), A method of analysis of the stability of embankments using parallel interslice forces, Geotechnique, Vol 17, pp 11-26.
[A3] D'Appolonia DJ, D'Appolonia E and Brisette RF (1968), Settlement of Spread footings on sand, Journal of Soil Mechanics and Foundations Division, Proc ASCE, Vol 94, No SM3, presented in Das BM (1983) Advanced Soil Mechanics, McGraw Hill, p 425.

the soil mass was subjected to additional horizontal and vertical acceleration $E_h g$ and $E_v g$ where g is the acceleration due to gravity. A positive value of horizontal acceleration is assumed to act in the direction which will decrease stability. The program automatically assumed a direction of vertical acceleration which minimised the factor of safety (calculated on soil strength).

Slope assumes strain compatibility. Clearly this will not be the case when the shear surface passes through a loose and a dense zone each of which will attain maximum strength for different strains. However since the analysis was qualitative this affect has been ignored.

A summary of the load cases and results is given in Table 24. Figures. 1 to 13 show the predicted slip surface for each analysis.